Saccades and pre-saccadic stimulus repetition alter cortical network topology and dynamics: evidence from EEG and graph theoretical analysis

Amirhossein Ghaderi [a,b]

ghaderi@yorku.ca

Matthias Niemeier [c,a,b]

John Douglas Crawford [a,b,d,e,f,*]

* Corresponding author: jdc@yorku.ca

[a] Centre for Vision Research, 4700 Keele St, ON M3J 1P3, York University, Toronto, ON, Canada,

[b] Vision Science to Applications (VISTA) Program York University, 4700 Keele St, ON M3J 1P3, Toronto, ON, Canada,

[c] Department of Psychology, University of Toronto Scarborough, 1265 Military Trail, Scarborough, ON M1C 1A4 Canada,

[d] Department of Biology, York University, 4700 Keele St, ON M3J 1P3, Toronto, ON, Canada,

[e] Department of Psychology, York University, 4700 Keele St, ON M3J 1P3, Toronto, ON, Canada,

[f] Department of Kinesiology and Health Sciences, York University, 4700 Keele St, ON M3J 1P3, Toronto, ON, Canada

Acknowledgements: We thank Dr. X Yan for technical support. This research was funded by the National Science and Engineering Research Council of Canada (NSERC). J.D. Crawford was supported by a Canada Research Chair. A. Ghaderi held a Vision: Science to Application (VISTA) Fellowship, supported by the Canada First Research Excellence Fund. M. Niemeier was supported by an NSERC Discovery grant.

Abstract:

Parietal and frontal cortex are involved in saccade generation, but their output signals also modify visual signals throughout cortex. These signals produce well-documented behavioral phenomena (saccades, saccadic suppression, various perisaccadic perceptual distortions) but their underlying influence on cortical network dynamics is not known. Here, we combined high resolution electroencephalography (EEG) with frequency-dependent source localization and graph theory analysis (GTA) to understand how saccades and pre-saccadic visual stimuli interactively alter cortical network dynamics in humans. 21 participants viewed series of 1-3 vertical or horizontal grids, followed by grid with the opposite orientation just before a horizontal saccade or continued fixation. EEG signals from the presaccadic interval (cue + 200ms, or equivalent fixation period) were used for source localization. Source localization (saccade – fixation) identified bilateral dorsomedial frontoparietal activity across frequency bands, whereas stimulus repetition produced band-specific modulations in left prefrontal, posterior parietal, and central-superior frontal and/or parietal cortex, with significant saccade-repetition interactions in frontal and parietal regions. GTA analysis revealed a saccade-specific functional network with major hubs in inferior parietal cortex (alpha) and the frontal eye fields (beta), and major saccade-repetition interactions in left prefrontal (theta) and supramarginal gyrus (gamma). Overall, quantitative measures of whole-brain network topology and dynamics (segregation, integration, synchronization, complexity) were enhanced during the presaccadic interval, but repetition interactions reduced synchronization and complexity. These results show that presaccadic signals have widespread, coherent influence on cortical network dynamics, likely responsible for both saccade production and the perceptual phenomena associated with saccades.

Highlights:

- Source localization & graph theory were used to analyze presaccadic EEG signals
- Presaccadic signals produced band-specific modulations/hubs in parietofrontal cortex
- Frontal/parietal eye fields showed extensive functional connectivity across all lobes
- Presaccadic stimulus repetition further modulated functional network connectivity
- Saccades and repetition both influenced network clustering, integration, & complexity

Keywords: Saccades, functional brain net work, integration, segregation, synchronization

Introduction:

Every day we perform thousands of saccades for purposes ranging from reading to looking at a landscape (Kleiser, Seitz, & Krekelberg, 2004). During each saccade, the eye rapidly moves to a new fixation point in order to maximize foveal vision (Bahill, Clark, & Stark, 1975; Harris & Wolpert, 2006). Thus, saccades are critical for vision, but they also produce challenges for vision, such as the need to suppress visual blur and integrate visual information across fixations (Bell et al., 2005; Melcher & Colby, 2008).) Thus, saccades and vision interact at various cognitive levels (Burr & Morrone, 2011; Eagleman, 2005; Morrone, Ross, & Burr, 2005; Ross et al., 2001). Consistent with this, saccade-related modulations are found throughout cortex (Barash et al., 1991; Berman et al., 1999; Chen & Crawford, 2017; Fairhall et al., 2017; Medendorp et al., 2007; Paré & Wurtz, 2001). But despite numerous studies on this topic in both animals and humans (summarized below), the motor and sensory influence of saccades on cortical network dynamics remains untested at the whole brain level.

Cortical saccade modulations can be roughly categorized into two categories, the first being their motor function. The cortical structures for saccade generation were first described in animals, including the parietal eye fields (lateral intraparietal sulcus; LIP) and the frontal/supplementary eye fields (FEF/SEF)), located in the lateral and medial prefrontal cortex respectively (Anderson et al., 1994; Barash et al., 1991; Hanes, Thompson, & Schall, 1995; Schall & Hanes, 1993). When a delay is interposed between visual stimulus appearance and the saccade (as in many behavioral paradigms) these areas typically show a visual response, followed by memory delay signals, and then ‘build up’ activity leading up to the saccade motor response (Powell & Goldberg, 2000; Sadeh et al., 2018; Sajad et al., 2016). Functional magnetic resonance imaging (fMRI) studies have confirmed the existence of human analogs to the frontal and parietal eye fields (Anderson et al., 1994; Berman et al., 1999; Levy et al., 2007; Vesia & Crawford, 2012).

The second type of saccade-related modulation in cortex relates to sensory processing. The motor signals described above are also thought to influence sensory processing, through corollary discharge (also known as ‘efference copies’). These signals are thought to suppress visual signals during saccades (Bremmer et al., 2009; Burr, Morrone, & Ross, 1994; Frost & Niemeier, 2015; Kovalenko & Busch, 2016; Shioiri & Cavanagh, 1989; Thiele et al., 2002), and second, to update or “remap” presaccadic signals so that they correctly align with post-saccadic visual input (Burr & Morrone, 2011; Duhamel, Colby, & Goldberg, 1992; Melcher, 2007; Sapir et al., 2004). Such signals (directly, or through their influence on vision) have been observed throughout occipital, parietal and frontal cortex neurons, just before and during saccades (Sommer & Wurtz, 2000; Duhamel et al., 1992; Nakamura et al. 2002; Kusunoki & Goldberg, 2003). Analagous saccade-dependent visual modulations of object location have also been observed in human fMRI studies (Merriam et al. 2007; Medendorp et al. 2003, 2005).

Finally, it is thought that the brain has specific neural mechanisms for integration of pre and post-saccadic object features (Burr & Morrone, 2011; Fabius et al,, 2020; Melcher, 2007; Prime et al. 2008, 2010). Consistent with this, some occipital and parietal areas, particularly the cuneus and the right supramarginal gyrus, show saccade-dependent interactions between pre- and post-saccadic stimulus features (orientation, spatial frequency) akin to repetition suppression / enhancement (Baltaretu et al., 2020; Dunkley, Baltaretu, & Crawford, 2016). These remapping, updating and integration signals are thought to be related to perceptual distortions that occur before, after, or across saccades (Binda et al., 2009; Burr et al., 2011; Eagleman, 2005; Morrone et al., 2005; Ross et al., 2001; Ghaderi & Crawford, 2020).

In summary, the visual and motor events associated with saccades, and their interactions, have been widely investigated in the local, regional, and behavioral levels, but the network topology and dynamics of this system have not been studied at the whole-brain level. Neurophysiology has high spatial and temporal resolution but is usually limited to local recordings. fMRI has whole-cortex capacity and reasonable spatial resolution, but its temporal resolution is too limited to isolate presaccadic vs.

post-saccadic effects. Magnetoencephalography (MEG) and electroencephalography (EEG) have high temporal resolution, but only recently have approached the spatial resolution of fMRI (Asadzadeh et al., 2020; Mégevand & Seeck, 2018; Wang et al., 2021). Previous EEG/MEG studies have shown that the phase and amplitude of different frequency bands may be altered in the perisaccadic interval (Busch, Dubois, & VanRullen, 2009; Fabius et al., 2020; Kovalenko & Busch, 2016; McLelland, Lavergne, & VanRullen, 2016; Medendorp et al., 2007; Staudigl et al., 2017), but did not study topology and dynamics of cortical networks constructed from correlated, source localized EEG signals.

A second technical barrier is the need for analytic tools that can quantify network dynamics at the whole brain level. Recently, various approaches in graph theoretical analysis (GTA) have been proposed in neuroimaging studies to investigate various aspects of functional brain networks (Bassett & Sporns, 2017; Ghaderi et al., 2020; Rubinov & Sporns, 2010; Sporns, 2014) (Note that functional connectivity refers to signal sharing / processing, it does not imply direct anatomic connectivity). In GTA, whole brain signal correlation patterns can be treated as functional networks composed of nodes (brain regions) and edges (a functional connectivity measure between pairs of regions). GTA can be used to derive various quantitative measures of functional network topology and dynamics (Bullmore & Sporns, 2009; Ghaderi, et al., 2020; Rubinov & Sporns, 2010; Stam, 2014), such as *clustering*, *efficiency, centrality, and energy* (see Table 1 for formal definitions and Methods for qualitative descriptions of these terms). These measures provide important quantitative information about functional network dynamics and topology, such as local vs. global connectivity, network stability, and uniformity of network connections (Bassett & Sporns, 2017; Ghaderi et al., 2020). To our knowledge, this approach has not been applied to the cortical saccade system, or its interactions with ambient visual signals.

Here, we combined high resolution EEG and GTA to study whole brain network topology and dynamics in the presaccadic period. Specifically, we tested the influence of an impending saccade on network dynamics in general, and its interaction with presaccadic visual processing. To test the latter, we employed a classic stimulus

repetition paradigm, (Grill-Spector, Henson, & Martin, 2006; Verfaellie et al., 2004), where visual stimuli were repeated, followed by the same/novel stimulus just before a saccade (Dunkley et al. 2016, Baltaretu et al. 2020). To probe interactions between presaccadic motor and visual signals, we employed the well-known effect of stimulus repetition on perception of a subsequent novel stimulus (Grill-Spector et al., 2006), by inserting this into the presaccadic interval (Ghaderi & Crawford, 2020). Based on previous EEG/MEG studies (Jerbi et al., 2009; Kovalenko & Busch, 2016; McLelland et al., 2016), we analyzed EEG sources in various frequency bands (i.e., theta, alpha, beta, and gamma bands). Then, we computed a functional connectivity measure (i.e., *lagged coherence*) between every pair of identified brain regions to construct functional brain networks and after that, various network properties, such as topology, complexity, and stability of synchrony were computed for these networks. We hypothesized that 1) saccades would alter local current density (related to neural activity) in the parieto-frontal regions discussed above, 2) these effects would interact with the influence of stimulus repetition on a pre-saccadic visual stimulus (Ghaderi & Crawford, 2020), and that 3) at the network level, saccades would increase synchronization and integration within a functional brain network that includes parieto-frontal hubs, but engages a much broader influence on cortical visual processing.

2- Method:

2-1 Participants and ethics approval. Twenty-one volunteers (12 females, aged between 18 and 44) participated in this study. All participants were right-handed and had normal or corrected to normal vision. We asked participants to report if they had a history of neuropsychiatric disorders or seizures and volunteers with positive history were excluded from the study. Each participant was paid 15 CAD/hour for participation. All participants signed an informed consent form that described all procedures about the experiment, data collecting/storage and analysis. This study was approved by the office of research ethics (ORE) at York University and the University of Toronto. All the methods in this study were performed in accordance with declaration of Helsinki.

2-2 Procedures and setup. A *saccade* and a *fixation* task were presented both during two separate sessions. In each session, participants were asked to perform both tasks

each day, and the order of tasks was counterbalanced across participants. For each participant, the second session was conducted one week after the first. During each session participants were seated in a dark room on a comfortable chair while we recorded their EEG and electrooculography (EOG) signals (controlled online by one author, A. G., from a separate room). Thirty-five centimetres in front of them a LED monitor (25”, refresh rate 144 Hz, full HD) presented stimuli programmed in MATLAB (ver. R2019a) using the Psychtoolbox-3 (version 3.0.16)(Kleiner, 2010; Kleiner, Brainard, & Pelli, 2007)

2-3 Stimuli and trials. Saccade and fixation trials were administered in different blocks. In saccade blocks (Fig. 1-a, left; also see Ghaderi & Crawford, 2020), trials started with the participant fixating a white cross (2 deg across) in the centre of a black screen and then pressing the space bar. After that, a reference stimulus appeared for 30, 50, 90, or 110 ms with its upper edge 5 deg (and its centre 11 deg) below the fixation point. The reference stimulus consisted of three white parallel lines (2° wide), separated by two 3° spaces, total size $12^o \times 12^o$) that were either all horizontal or vertical. For a third of the trials the stimulus appeared only once. Another two thirds of trials had the stimulus reappear for a second and third time, respectively, with a temporal gap of 300 ms between appearances. Two hundred milliseconds after the last presentation of the reference stimulus the fixation cross jumped 10 deg randomly to the left or to the right (the total number of saccades to the left and saccades to the right was equal). After 100 ms, and before the participant was able to move their eyes, a test stimulus appeared for 70 ms (Figure 1-b). The test stimulus was identical to the reference stimulus, except the lines were rotated by 90 deg (i.e., they were vertical when the reference lines were horizontal and vice versa). After the saccade, a blue square was presented at the center of screen and participants dragged the square with a mouse to judge whether duration of the test stimulus was longer (dragging up) or shorter (dragging down) than the last reference stimulus. The configuration of the tasks in this study was similar to our previous psychophysics and modeling study that was performed with longer intervals and vertical saccades (Ghaderi & Crawford, 2020). In total 720 saccade trials were collected across the two sessions. Another 720 fixation trials were collected where

stimuli and procedures were the same except the fixation cross always remained in the centre of the screen (Fig. 1-a, right side).

2-4 Saccade measurement and exclusion criteria. A schematic of the time course of saccades relative to other events is shown in Figure 1-b. EOG signals were recorded at 2048 Hz using a BioSemi System. Horizontal eye movements were monitored with bipolar EOG electrodes to the left and right sides of right eye. Vertical eye movements and blinks were detected using another electrode pair above and the eye. To distinguish microsaccades or drift from acceptable saccades, a calibration session for saccade amplitude was performed before the main experiment. In this session participants were asked to execute a 10° saccade to the left or right side (by changing the location of a fixation point on the screen). The mean change of amplitude in the EOG was calculated for 20 of these saccades. 70% of this mean was used as the minimum amplitude for saccades in the experimental data. Two other criteria for saccade exclusion were duration and latency (the time between shifting the location of fixation point and saccade onset). Saccade onsets and offsets were determined through visual inspection of the slopes of the EOG signals. Eye movements that took longer than 100ms (corresponding to a mean speed less than 100°/second) were excluded. Likewise, saccade latencies that did not fall between 200-450ms were excluded. Trials that included blink artifacts were excluded.

2-5 EEG acquisition, preprocessing, and extraction of event related signals. EEG acquisition was performed at 2048 Hz with a BioSemi system (ActiveTwo: DC amplifier, 24-bit resolution) via a high-density 64 EEG montage. All electrodes were referenced to a Common Mode Sense (CMS) active electrode and a Driven Right Leg (DRL) passive electrode (see http://www.biosemi.com). During the recording sessions, the impedance between electrodes and scalp was kept under 5 kilohms. An online anti-aliasing first order analog filter and an online fiftth order lowpass filter (<134 Hz) was applied by the BioSemi amplifier (see: http://www.biosemi. com/faq/adjust_filter.htm). The acquisition program was the Actiview program that is an open-source program written in LabVIEW (The National Instruments Inc.).

After recording, EEGs were imported to the MATLAB 2019a by EEGLAB toolbox (https://sccn.ucsd.edu/eeglab/index.php) and this toolbox was used for EEG preprocessing. A fift^{h} order bandpass digital filter (0.1 to 40 Hz) was applied. The duration of each EEG segment was 200ms, temporally centered on the onset of the test stimulus in both the fixation and saccade condition. Since the saccade cue occurred 100ms before the test stimulus, and mean saccade latency was 263.7ms (±41.4ms SD), this EEG segment fell within the presaccadic interval of the saccade trials (Figure 1b). Also note that since this EEG segment preceded the actual saccade artifacts related to eye dipoles orientation change and muscle contraction were minimized (Jerbi et al., 2009; Keren, Yuval-Greenberg, & Deouell, 2010). To remove any remaining artifacts from signals, the channel statistics approach in EEGLAB (https://eeglab.org/tutorials/06_RejectArtifacts/cleanrawdata.html) was used and single channels with continuous artifacts were excluded. In this approach, flat channels, channels with large amount of high frequency noise (based on their standard deviation), and channels that exhibited very low linear correlation with their nearby channels were removed. Then, signals were visually inspected and trials with obvious biological or technical artifacts i.e., muscle activity, head movement, eye blinks, irrelevant eye movements (see *Saccade measurement and exclusion criteria*) or other high amplitude artifacts with unknown sources, were excluded from the analysis.

2-6 Excluded participants and channels. Participants with more than 60% false trials (according to both EEG and saccade criteria) were excluded from the study. In the remaining participants, there was no significant difference in percentage of excluded trials between the *saccade* task (mean: 32.3, SD=10.8) and the *fixation* task (mean= 21.9, SD=7.1). Some EEG channels had to be eliminated (because of continuous artifact, bad channel, or dead channel) in some participants. These were channel PO4 for participants #8, #13, #14, #18, channel P9 for participant #3, #14, channel TP7 for participant #17, and channel CP6 for participant #11. The excluded channels were eliminated form both tasks to equalize number of channels among conditions.

2-7 sLORETA source localization. The clean EEG segments were imported to the LORETA software (version 20190617) (http://www.uzh.ch/keyinst/loreta) and EEG source

localization was performed in the frequency domain (cross-spectrum analysis) according to instantaneous discrete and linear solutions for the EEG inverse problem (Pascual-Marqui, 2002). LORETA computes EEG current density in 2394 gray matter cortical voxels and these voxels are grouped in 84 ROIs based on the boundaries of Brodmann areas (BA) for human cortex in Talairach coordinates. In this study we selected all these regions which contain BAs 1-11, 13, 17-25 and 27-47 in both hemispheres. Sources for the theta (4-8 Hz), alpha (8-12 Hz), beta (12- 28 Hz), and gamma (28-40 Hz) bands were calculated by the standard LORETA (sLORETA) algorithm (Pascual-Marqui, 2002). Current density in these sources was compared between conditions. After that the connectivity between sources was calculated for graph theory analysis.

2-8 Lagged coherence and adjacency matrix. To quantify functional connectivity between brain regions, we investigated oscillatory activity of current densities in different cortical regions using sLORETA-based *intracortical lagged coherence*. *Intracranial lagged coherence* between all pairs of EEG sources (localized based on the Brodmann areas described in section 2-7) was computed in different frequency bands in sLORETA (Pascual-Marqui, 2007). According to this procedure, *lagged coherence* between two multivariate timeseries (here, oscillations of current densities in two cortical regions) in a specific frequency band ($i.e., X_\omega, Y_\omega$; *where* ω *is frequency*) is defined as:

$$Lagged\ Coherence = \sqrt{\frac{Im\left[S_{xy}(\omega)\right]^2}{S_{xx}(\omega)S_{yy}(\omega) - Re\left[S_{xy}(\omega)\right]^2}} \qquad \text{eq. 1}$$

Where, *Im* and *Re* stand for the imaginary and real parts of Fourier transforms, respectively. $S_{xy}(\omega)$ is cross-spectral density between X_ω and Y_ω, and $S_{xx}(\omega)$ and $S_{yy}(\omega)$ are auto-spectral density for X_ω and Y_ω, respectively(Pascual-Marqui, 2007; Pascual-Marqui et al., 2011).

Intracortical lagged coherence is a modified version of instantaneous coherence that removes effects of volume conduction (Ghaderi, et al, 2018a; Pascual-Marqui et al., 2011). Volume conduction in EEG is generated by instantaneous changes in local field potentials and is related to electromagnetic induction in the brain tissue instead of

connectivity via neural circuits (Nunez et al., 1997). The effects of volume conduction are thought to be associated with the real part of coherence in Fourier transform (Pascual-Marqui et al., 2011). In calculation of *lagged coherence,* imaginary part of Fourier transform is considered, and the real part is removed (eq. 1). In this way, the effect of volume conduction in connectivity between regions is minimized.

2-9 Functional brain networks: topological indices, energy, and entropy.

In most brain network studies, brain regions are considered as nodes and the structural or functional relations between brain regions are treated as edges. Studies that describe physical pathways (i.e., white matter) between regions deal with *structural brain networks* and studies that only consider the linear/nonlinear relationships between neural activity in different regions describe *functional brain networks* (Rubinov & Sporns, 2010). In a *weighted network*, the values of these relationships vary continuously. Here, we investigated weighted functional brain networks in several conditions (e.g., saccades vs. fixation, stimulus repetition). To model these networks, each brain region (84 Brodmann areas), was treated as a node and the *intracortical lagged coherences* (as a measure of functional connectivity) between pairs of node were treated as *edges* (Bullmore & Sporns, 2009; Ghaderi et al., 2018a; Jouzizadeh, et al., 2021). Lagged coherence was computed for each participant, condition, and frequency band. These values were then arranged in an *adjacency matrix*. In the adjacency matrix, each row / column represents one region, and the intersection of rows and columns represents the value of the *lagged coherence* between these two regions. We normalized these values to obtain consistent (weight conserving) GTA measures across conditions (Rubinov and Sporns 2011). This ensures that GTA indices are independent of the distribution of matrix weights. These adjacency matrices were used for further analysis using conventional and spectral graph theoretical approaches to obtain topological and dynamical features of functional brain networks.

2-9-1 Topological features of functional brain networks

Conventional GTA indices were used to describe the topology of functional brain networks (Bullmore & Sporns, 2009; Rubinov & Sporns, 2010). Topological features in a complex network are characterised by the architecture of the paths between nodes,

considering all nodes and edges. We used the three topological features that are most commonly used to describe human brain networks: *segregation*, *integration,* and *centrality* (Bullmore & Sporns, 2009; Rubinov & Sporns, 2010; Deco et al., 2015; Ghaderi et al., 2018b, 2019; Kitzbichler et al., 2009; Rubinov & Sporns, 2010; Sporns, 2013). These network features are described qualitatively in the following paragraphs (see Table 1 for formal mathematical definitions).

Functional segregation is related to the presence of highly interconnected nodes via local circuits, i.e., *modules* (Rubinov & Sporns, 2010). Networks with the capacity for local / modular processing are considered to be segregated networks. Several studies have suggested that functional brain networks are segregated networks (Bassett & Bullmore, 2007; Bullmore & Sporns, 2009, 2012; Watts & Strogatz, 1998). In functional network analysis, the c*lustering coefficient (CC)* is often used to measure the level of segregation (Bialonski & Lehnertz, 2013; Deco et al., 2015; Ghaderi et al., 2018b; Pedersen et al., 2015; Rubinov & Sporns, 2010; Sjoerds et al., 2017). The clustering coefficient is calculated for each node and the average *CC* for all nodes is used to quantify the overall level of functional segregation in the network. For each node, *CC* is related to number of clusters around the node. In this study, clusters are defined as 'triangles', i.e., triplets of interconnected neighbour nodes. In a weighted network, when the neighbors of a node all have maximum connection weights, *CC* is maximum and equals 1, whereas *CC* equals 0 if the node has no connections.

Functional integration is related to combination of information across distributed network nodes, and indicates the level of global information processing (Rubinov & Sporns, 2010). Several studies have shown that functional brain networks are highly integrated and exhibit very fast integration between distributed anatomical regions (Bassett & Sporns, 2017; Bullmore & Sporns, 2012; Rubinov & Sporns, 2010; Stam, 2014; Stam & Reijneveld, 2007). Functional integration in brain networks can be affected by alterations in brain states, diseases or disorders (Ghaderi et al., 2017, 2020; Hasanzadeh et al., 2020; Rubinov & Sporns, 2010; Stam & Reijneveld, 2007; van den Heuvel et al., 2008). In GTA, functional inegration can be measured by *global efficiency* (*Ef*), which is inversely proportionate to the average highest weights between all pairs of

nodes (Boccaletti, et al., 2006; Newman, 2008; Rubinov & Sporns, 2010). In a network where all node pairs are highly connected, path lengths are called 'short' and thus information can be transferred rapidly. Such networks have high global efficiency, i.e., high levels of integration (Boccaletti et al., 2006; Newman, 2008).

Networks with high values of both *CC* (clustering) and *Ef* (integration) are known as *small world* networks. Such networks display fast and efficient information processing. Many studies have suggested that brain networks are small-world networks (Bassett & Bullmore, 2006; Ghaderi et al., 2018a; Muldoon et al., 2016; Watts & Strogatz, 1998). Small-worldness in functional brain networks is affected by both specific cognitive states (G. Li et al., 2019; Lin et al., 2018) and brain diseases / disorders (Jouzizadeh et al., 2021; Lynall et al., 2013; Stam, 2014). *Small-world propensity (SW*) has been used to evaluate small-worldness in functional brain networks (Muldoon et al., 2016). SW is calculated by taking the ratio of *CC* and *Ef* in the experimental brain network in comparison to these measures in control networks (i.e., random and regular networks), where higher SW values indicate higher small-worldness (Muldoon et al., 2016).

Finally, *centrality of nodes* is used to evaluate the importance specific nodes. Nodes that are connected to many other nodes are called 'important'. Nodes that have many connections to important neighbors are called hubs. Hubs can be defined mathematically (Table 1) as nodes with the highest *Eigenvector centrality* (Eig_C) values (Fagerholm et al., 2015; Ghaderi et al., 2021; Joyce et al., 2010). In functional brain networks, alteration of Eig_C suggests that the node's contribution to the whole network has changed. Here, we compared Eig_C of all brain regions in different conditions to find which regions were most important for different brain networks, for example during saccades versus fixation.

All these topological indices were calculated using *Brain Connectivity Toolbox* (Rubinov & Sporns, 2010) (https://sites.google.com/site/bctnet/).

2-9-2 Synchrony and complexity of functional brain networks

Note that in EEG data, each time series measurement takes the form of an oscillation, and the entire set of measurements can be considered an oscillatory system. For such

systems, each oscillatory unit can be treated as a node and the level of similarity between oscillations across nodes as the edge. A subfield of GTA, known as *spectral graph theory*, is devoted to evaluate stability of synchronizations and robustness of oscillatory systems (Spielman, 2007; Wilf, 1967). In spectral graph theory, *stability of synchronization* (i.e., the level of coupling between all dynamical nodes) can be evaluated by employing linear algebra and investigating the eigenvalue spectrum of the adjacency matrix (Atay et al, 2006; Larremore et al., 2011; Spielman, 2007). The sum of all eigenvalues of the matrix is called *energy of graph (H*), and is directly related to the stability of synchronization in the system (Gutman, 2013; Li et al., 2012). Here, we used *H* to evaluated stability of synchronization in our EEG data (Ghaderi et al., 2020, 2021). Previous studies showed that when all nodes in a network show high synchronization (coupling) during a specific period, then the network exhibits a high value of *H* (Daianu et al., 2015; Amir Hossein Ghaderi et al., 2020; Gutman & Zhou, 2006). In this study, we calculated *H* using the *eig* function (MATLAB R2019) for each adjacency matrix and then compared this value across conditions and participants.

To investigate *network complexity* (the variety of connections among nodes) in our functional brain networks, Shannon entropy (*S*) of networks were compared between conditions (Ghaderi et al., 2019, 2020). The value of *S* is directly related to the number of possible states for a probability system (e.g., *S* is higher for dice rolling than a coin toss). For an adjacency matrix (with many possible connectivity states between nodes), *S* is higher in the presence of more variable connection weights. *S*=0 when all values of connections are same, whereas it increases in presence of rare values, called 'surprise states' (Ghaderi et al., 2019, 2020, 2021). In a functional brain network, surprise states occur for brain functions that require high coupling between two specific nodes (Ghaderi et al., 2019, 2020, 2021). In this study we used the *entropy* function (MATLABR2019) to compute *S* for all adjacency matrices (again, see Table 1 for mathematical details).

2-10 Statistical analysis. In this study we aimed to investigate 1) the brain regions and network properties associated with the presaccadic signal processing, and 2) how these properties were modulated by repetition of a presaccadic reference stimulus, in a task where participants had to judge the duration of a subsequent perisaccadic visual

stimulus. To this aim, four conditions were assumed. 1) The *saccade* condition i.e., trials in the *saccade* task that were presented with 0 repetitions of the reference stimulus. 2) The *fixation* condition i.e., trials in the *fixation* task that were presented without repetition of the reference stimulus. 3) The *saccade/repetition* condition i.e., trials in the *saccade* task that were presented repetitions of the reference stimulus, combined for statistical power because they did not produce different effects in a preliminary psychophysical study (Ghaderi and Crawford 2020) 4) The *fixation/repetition* condition i.e., trials in the *fixation* task that were presented with one or two repetitions of *reference*.

To compare brain activity among the different conditions, a *cluster-based nonparametric permutation t-test*(Maris & Oostenveld, 2007) was performed to find significant differences of current densities within Brodmann areas. For each *cluster-based nonparametric permutation t-test,* 10000 random shuffles were implemented. The network indices were compared using the separate *nonparametric permutation t-test* (10000 random shuffles and significance level<0.05) among conditions. The sources of activity and network indices of these pairs of conditions were compared: *saccade* vs. *fixation, saccade/repetition* vs. *saccade,* and *fixation/repetition* vs. *fixation.* Then, to correct the induced error of multiple comparisons (error type 1), false discovery rate (FDR) analysis was performed and corrected p-values under 0.05 were considered significant. These analyses were performed in various frequency bands. The nonparametric cluster-based permutation t-test and FDR analysis were performed using MATLAB 2019a.

3- Results:

To evaluate neural processes associated saccade preparation, high-density EEG data from the presaccadic interval of the *saccade task* were compared to data from the same time segment in the *fixation* task (see method section and Figure 1 for more details). To test how these signals interact with presaccadic visual processing, this time interval incorporated the presentation of a test stimulus and was preceded by a single or repeated presentation of a reference stimulus (Figure 1). Thus, we considered the presaccadic interval under four conditions: *Fixation (F), Saccade (S),* both after a single presentation of the reference stimulus, as well as *Fixation/Repetition (FR),* and

Saccade/Repetition (SR) conditions. In the following two sections we begin with source localization analysis, using fairly standard neuroimaging conventions, followed by a functional network analysis based on GTA. Each of these sections is broken down into four subsections: saccade effects, stimulus repetition effects, their interactions and then post-hoc analysis. Table 2 provides the functional anatomy and coordinates of Brodmann areas mentioned in the text.

3-1 Source localization

3-1-1 Saccade vs. fixation: False discovery rate (*FDR*) analysis indicated significant differences of clustered voxels between the *Saccade* and *Fixation* conditions, i.e. [(SR +S) – (FR + F). In all regions and all investigated frequencies, the current density was decreased in the *saccade* condition in comparison to the *fixation* condition (Figure 2). The statistical values of these differences are shown in Table 3. This analysis yielded significant differences for t-values higher than 4.321 in the theta, 5.540 in the alpha, 4.535 in the beta, and 4.405 in the gamma bands (Table 3). Current modulations tended to peak near the medial portions of superior frontoparietal cortex, especially in the theta and gamma bands. After *FDR* analysis and according to the sLORETA map, significant differences were observed in BAs 5, 7, 8, and 46 (Figure 2; Table 2). According to standard coordinates (Table 2), areas 8 and 46 correspond to the frontal eye fields and dorsolateral prefrontal cortex. A large area of saccade modulation was also observed in posterior parietal cortex (PPC) spanning the superior and medial portions of Brodmann's areas 5 and 7, i.e., dorsal posterior parietal cortex, including the medial portion of PPC (precuneus). In other words, this large region of modulation spanned sites associated with saccade production (Hanes et al., 1995; Hanes & Wurtz, 2001; Paré & Wurtz, 2001) to more medial regions associated with complex visuospatial processing (Chen & Crawford, 2017; Chen et al., 2018).

3-1-2 Repetition vs. no repetition:

Previous studies have shown that repetition of a visual stimulus alters perception of a subsequent novel test stimulus (which fell within the EEG analysis window of the current study). Here, we used this paradigm as a probe into presaccadic visual signal processing. We first tested the main influence of stimulus repetition on the combined

saccade/fixation dataset, i.e., [(SR + FR) – (S + R)]. Based on nonparametric permutation t-tests, significant differences between the *repetition* condition and the *no-repetition* conditions were only observed in the beta band (t-value=-8.37, |t-value|>4.321 was significant) and were confined to clustered voxels of BA 7 (dorsal posterior parietal cortex). In this band/region, current density was lower in the repetition condition (Figure 3). We next tested interactions between this effect and saccades, to directly probe the influence of presaccadic signal processing on simultaneous visual processing signals.

3-1-3 interaction of saccade and repetition effects: To directly test the interaction between saccade and repetition effects, we compared current densities as follows: (*Saccade/repetition* minus *Saccade* condition) minus (*Fixation/repetition* minus *Fixation* condition), i.e., [(SR-S) – (FR-F)} (Figure 4). Cluster-based permutation tests and FDR analysis showed significant differences in t-values higher than: 3.721 in the theta, 4.321 in the alpha, 4.535 in the beta, and 4.321 in the gamma bands. Based on these analyses significant differences were observed in bilateral BA 7 (all frequency bands), including the superior parietal cortex and precuneus regions (Figure 4). The statistical details of these results are presented in Table 3.

3-1-4 Post hoc analysis: influence of stimulus repetition in the presaccadic interval: In a post hoc analysis we analysed FR-F and SR-S separately. First, we removed all saccade trials to compare *fixation-repetition* (FR) and *repetition* (R) trials. According to the *FDR* analysis, we observed no significant difference between trials with repetition and without repetition of reference stimulus. However, in the *saccade* task (SR – S), the *FDR* analysis showed significant differences in neural activity for clustered voxels between the *saccade/repetition* condition and the *saccade* condition (Figure 5). In this case, stimulus repetition sometimes resulted in either reduced (blue) or increased (orange) current density, depending on the region and band. The *FDR* indicated t-values higher than 4.321 in the theta, 4.321 in the alpha, 5.540 in the beta, and 4.535 in the gamma bands (Table 3). The significantly increased current density in the *saccade/repetition* condition (in comparison to the *saccade* condition) was observed in Brodmann areas 3 (beta band), and 7 (gamma band) in both hemispheres (Figure 5). BA 3 includes the postcentral gyrus and BA 7 (posterior parietal cortex) including the

precuneus (Table 2). A significantly decreased current density (in the *saccade/repetition* condition compared to the *saccade* condition) was observed in left Bas 8, 46 (theta and gamma bands) and bilateral BA 7 (theta and alpha bands) (Table 3). BAs 8, 46 span superior and medial frontal gyrus including the FEF. The statistical details of these results are presented in Table 3. In short, these modulations again spanned parieto-frontal areas associated with saccades and higher level visual / executive function (Leoné et al., 2014).

Overall, the regions of modulation observed in this study were consistent with those observed in fMRI studies of saccades (Alkan et al., 2011; Berman et al., 1999; Dunkley et al., 2016; Fairhall et al., 2017). However, source localization analysis is limited in terms of understanding the functional connectivity between these regions and with other areas of cortex in this task.

3-2 Network Analysis:

For the next stage of our analysis, we re-examined the data using graph theoretical analysis (GTA). By this analysis we can test the architecture and dynamics of functional connectivity patterns in whole brain network in presaccadic interval. To quantify network topology and dynamics we computed the following GTA measures: 1) *eigenvector centrality (Eig_C)* to identify important nodes and hubs, 2) *clustering coefficient (CC)* to represent the degree of segregation of the network into local clusters, *3) global efficiency (Ef)* to represent integration of signals across the network, *4) small-worldness (SW)* to represent the overall efficiency of the network at both local and global levels, 5) energy (H) to represent stability of synchronization in the network, and *5) entropy (S)* to determine the complexity of the network (see Methods sections 2.8, 2.9 for qualitative explanations and Table 1 for formal definitions of these terms). Then these values were statistically compared between conditions by permutation tests and the *FDR* approach for multiple comparisons correction. Following the same order as the source localization analysis in the previous section, we used this approach to examine functional connectivity for Saccades vs. Fixation, Stimulus Repetition vs. no Repetition, and their Interactions.

3-2-1 Saccade vs. fixation: Figure 6 shows the anatomic distributions of network nodes that exhibited significant differences of *eigenvector* centrality (Eig_C) in the *saccade* minus *fixation* condition, based on FDR analysis in the alpha and beta bands. In other words, this figure shows brain areas with increased functional connectivity just before a saccade. In this figure, *small black dots* indicate the sites tested and the *blue-green lines* indicate functional connections that were stronger in the saccade condition (only the top 20% are shown). The *large red dots* indicate hubs with significant differences of centrality, and the functional connections of these particular nodes are highlighted in red. In the alpha band, BA 39 (left hemisphere) (t=2.21, p=0.04) was a significant hub. BA 39 includes angular gyrus and supramarginal gyrus (SMG). This area was more widely connected to the frontocentral and occipital regions just before saccades. In the Beta band, significant differences of Eig_c were observed in BA 8 (both hemispheres) (left: t=3.31, p=0.004; right: t=2.46, p=0.024) that includes FEF). These regions were more widely connected to the prefrontal and temporoparietal regions (right hemisphere) and centroparietal regions (left hemisphere). In short, this analysis revealed hubs in brain areas associated with saccade production and trans-saccadic integration), and their functional connections to occipital, parietal, and frontal cortex during this particular task (Baltaretu et al., 2020).

Whereas Figure 6 only illustrated nodes and connectivity for specific frequency bands, Figure 7 shows how five more general GTA measures changed in the saccade condition, across all bands analyzed. Each 'violin plot' shows the distribution of values across all participants for a given GTA measure (columns CC, Ef, SW, H, Entropy) and frequency band (rows theta, alpha, geta, gamma). Significant increases (*/**) in the clustering coefficient (CC) and in global efficiency (EF) suggest greater local and global connectivity, respectively, in presaccadic functional networks. Furthermore, the presaccadic interval was associated with a higher degree of synchronization stability and complexity, as measured by energy (H) and Shannon entropy (S). Only the measure of small-worldness (SW) remained unchanged. (See Figure Legend 7 for Statistical Values).

3-2-2 Stimulus Repetition vs. no repetition: main effect and interaction with saccades. The combined saccade/fixation dataset only showed one significant main effect for repetition vs. no repetition: significantly higher clustering coefficient for the no-repetition condition (t=1.86, p=0.047) in the beta band. However, several significant interactions were observed between repetition and saccade effects.

Figure 8 shows the anatomic distribution of network nodes with significant differences of Eig_C between *fixation/repetition* minus *Fixation* (*FR-F*) and *saccade/repetition* minus *Saccade* (*SR-S*) according to FDR analysis in different bands. In other words, brain areas where saccade plan and stimulus repetition interacted to influence functional connectivity in the presaccadic interval. This figure follows the same conventions as Figure 6.

In the theta band, left BAs 44 (t= 3.86, p=0.001), 45 (t= 4.28, p<0.001), 46 (t= 2.9, p=0.01) showed significant differences of Eig_C. These regions include inferior frontal and dorsolateral prefrontal cortex. These regions were densely connected to temporoparietal regions. Furthermore, in this band, a significant difference in Eig_C was also observed in the right BA 7 (t= 3.11, p=006), including precuneus. This region showed functional connectivity with frontoparietal regions. In the alpha band, significant differences of Eig_C were observed in right BA 7 (t=2.31, p=0.033). This region exhibited connectivity with frontoparietal regions. In the Beta band, significant differences in Eig_c were found in left BAs 3 (t=2.83, p=0.012), 8 (t=3.48, p=0.003), 19 (t=3.74, p=0.002) (a part of visual cortex) and right BA 9 (t=3.14, p=0.006) which is part of the medial and dorsolateral prefrontal cortex. In this band the connectivity pattern was complex, with widely connections from these areas to other brain regions. Finally, in the gamma band, significant differences in Eig_C were observed in left Brodmann 40 (t= 2.55, 0.021) (which includes SMG) and right BA 19 (t=2.80, p=0.003) which is a part of the occipital lobe. In this band left SMG (BA 40) exhibited connectivity to frontal and occipital regions and right visual cortex showed connectivity to temporal and frontal regions.

Figure 9 shows the distribution of each network measure across individuals in different bands for the interaction [(SR-S) – (FR-F)] comparison, using the same conventions as Figure 7. Here, between SR-S and FR-F, the clustering coefficient *(CC), Global*

Efficiency (Ef), Energy H, and entropy (S) were significantly different. In the *SR-S*, the clustering coefficient and global efficiency were higher, and energy and entropy were lower in comparison to the *FR-F* (see Figure legend 10 for statistical details).

3-2-3 Post hoc analysis: influence of stimulus repetition in the presaccadic interval.

A post hoc analysis was performed for separate trials in the *saccade* and *fixation* tasks. After removing the saccade data, no significant differences remained between Eig_C values in the *Fixation* condition and *fixation/repetition* condition. However, several significant differences were observed between the *saccade/repetition* and the *saccade* conditions in the network features. Figure 10 shows these differences using the same analysis and conventions as Figures 6 and 8. In the Theta band, Eig_C was significantly repetition-dependent in the right BA 7 (t=3.25, p=0.004) which includes precuneus, with connections to frontoparietal cortex. In the alpha band, right BA 39 (t=3.09, t=0.007), containing angular gyrus and SMG, also connected to frontoparietal cortex. In the gamma band, several significant hubs showed up, including left BA 40 / SMG (t=2.42, t=0.027), right BA 46 / dorsolateral prefrontal cortex (t=0.013, p=0.013), area 17 / primary visual cortex. etc. Each of these areas showed diffuse functional connectivity in this band. Overall, this comparison engaged areas related to low-level vision, high-level vision, and saccades, with widespread functional connectivity throughout cortex.

Figure 11 shows the graph measure distributions the SR-S Comparison, using similar conventions to Figures 7 and 9. In the alpha band, the entropy was significantly lower in the *saccade/repetition* condition in comparison to the *saccade* condition (t=2.34, p=0.032) that means the complexity of functional brain network was decreased in the *saccade/repetition* condition. In the Beta band, the *CC* (t=2.35, p=0.031), and the *Ef* (t=2.34, p=0.032) were significantly higher in the *saccade/repetition* condition while the *S* was significantly higher (t=2.72, p=0.014) in the *saccade* condition. This suggests increased integration and segregation but decreased complexity in the *saccade/rep*etition condition. In the gamma band, the results were similar to the alpha band and *S* was significantly higher in the *saccade* condition (t=2.09, p=0.040) in comparison to the *saccade/repetition* condition. This result also suggests decreased

complexity in the *saccade/rep*etition condition. Briefly, these results reveal that repetition of a pre-saccadic stimulus can increase the segregation and integration of functional brain networks but decreases complexity in these networks.

4- Discussion

EEG / MEG have been employed previously to identify fast neural responses in the presaccadic interval (Forgacs et al., 2008; Jerbi et al., 2009; Kern, Schulze-Bonhage, & Ball, 2021; Kovalenko & Busch, 2016; McLelland et al., 2016; Medendorp et al., 2007), but this study introduced several innovations: first, the addition of pre-saccadic stimulus repetition to probe saccade-vision interactions, second, the use of EEG source localization, and third the use of GTA to quantify functional bran network topology/dynamics. Overall, our results show that during the presaccadic interval, saccades caused modulations in dorsomedial parietofrontal cortex, with decreased current density in all four frequency bands (theta, alpha, beta, gamma) and prominent connectivity in BA 8 (frontal eye fields) and 39 (inferior parietal cortex) in the alpha and beta bands. Presaccadic stimulus repetition interacted with the saccade-fixation at both local and network levels, with increased bilateral precuneus current density and highly increased connectivity for a number of band-specific hubs. Post-hoc analysis revealed that this was primarily due to presaccadic interactions with motor signals in the saccade condition, where repetition decreased frontoparietal current density in the alpha and beta bands and increased network connectivity in various hubs. Importantly, saccades and stimulus repetition both produced enhanced network segregation and integration, although they had opposite effects on entropy. In the following sections we discuss and interpret these results in more detail.

4-1 Functional anatomy of presaccadic signals in frontoparietal cortex

Previous neurophysiological and neuroimaging studies have implicated superior and medial frontal cortex (specifically FEF/SEF respectively) and parietal cortex (especially monkey intraparietal cortex) in saccade planning and remapping ((Anderson et al., 1994; Barash et al., 1991; Schall & Hanes, 1993; Schall et al., 1995; Umeno & Goldberg, 1997)). Our source localization analysis showed reduced current density (in all frequency bands) in dorsomedial frontal cortex and the superior parietal lobule. Note

that reduced current density has been associated with desynchronization, and thus greater complexity of neural activity (Blohm et al., 2019). These results are consistent with previous studies showing alpha and beta desynchronization in superior/medial frontal regions and superior parietal cortex during saccades and other actions (Brignani et al. 2007; Leocani et al.; 1997; Stancák & Pfurtscheller, 1996; Tzagarakis et al. 2010).

Prefrontal regions of presaccadic current density modulation included 1) the classic frontal eye fields (Anderson et al., 1994; Schall & Hanes, 1993), 2) more medial areas that could contain dorsolateral prefrontal cortex (DLPFC), a saccade-modulated area involved in working memory and executive functions (Balan & Ferrera, 2003; Takeda & Funahashi, 2002). We also observed altered presaccadic current density in the medial posterior parietal cortex (precuneus). Precuneus is not considered part of the classical oculomotor system, but is activated in tasks that involve perisaccadic processing of multiple, complex visual stimuli (Chen et al., 2018; Frings et al., 2006). Precuneus activation may have been associated with additional demands in our particular task, such as the increased difficulty of judging stimulus duration in the presaccadic interval (Gitelman et al., 1999; Huddleston et al., 2021; Mort et al., 2003).

Likewise, our network analysis identified major presaccadic ‘hubs’ (i.e., sites that show a high degree of functional connectivity with other well-connected sites) in bilateral BA 8 (in the beta band) and left BA 39 (in the alpha band). BA 8 encompasses the FEF, and BA 39 includes the regions of posterior parietal and especially angular gyrus. Angular gyrus has previously been implicated in saccade memory / planning and may be part of the human expansion of the monkey parietal eye fields (Vesia & Crawford, 2012; Vesia et al., 2010). These results generally overlapped with our source localization results, but whereas the latter included more medial peaks (associated with ‘cognitive’ areas), GTA tended to highlight more lateral sites associated with saccade production (Vesia & Crawford, 2012). This could arise because current densities are driven by local processing whereas connectivity analysis is more influenced by longer-range transmission of motor signals. It should also be noted that these results were frequency band dependent. For example, medial parieto-frontal current densities showed strongly in theta and gamma bands associated with memory (Kawasaki & Yamaguchi, 2013;

Pesaran et al., 2002), whereas presaccadic hubs showed best in alpha and beta bands associated with sensorimotor activity (Buchholzet al., 2014).Taken together, our source and GTA results suggest that human frontal and parietal eye fields show both greater activity and connectivity just before a saccade, consistent with their known role in saccade generation and high-speed neural signal transmissions in presaccadic interval.

4-2 Functional network features in the presaccadic interval:

The presaccadic network hubs described above showed extensive connectivity throughout the brain, with major ipsilateral connections in the beta band from Brodmann area 8 (FEF) to superior posterior parietal cortex and other frontal regions (Figure 6). Brodmann area 39 (inferior parietal cortex) showed extensive bilateral connectivity in the alpha band with various frontal lobe regions implicated in saccade processing (Anderson et al., 1994; Funahashi et al., 1991) as well as contralateral parietal cortex. Although functional connectivity does not necessarily imply direct anatomic connection, this is consistent with the known anatomic connections between parietal and frontal saccade areas, and likely involves both feedforward and recurrent processing of saccade planning signals (Alkan et al., 2011; Andersen et al., 1990; Anderson et al., 1994; Corbetta et al., 1998).

Besides providing measures of specific connectivity, GTA analysis provides global quantitative indices of functional network topology, such as clustering coefficient (*CC*), and efficiency (*Ef*), all of which increased here in the period before saccades. The *CC* and the *Ef* in the functional brain networks are associated with network segregation and network integration, respectively (Bullmore & Sporns, 2009; Ghaderi et al., 2017, 2018b). Higher values of the *CC* exhibit higher level of information processing in the local circuits whereas higher values of the *Ef* indicate faster information propagation in the large scale brain network (Rubinov & Sporns, 2010). Networks with high values of the *CC* and the *Ef* are efficient networks for information transformation in the local and global levels (Watts & Strogatz, 1998; Rubinov & Sporns, 2010). Thus, network segregation and integration increased in the presaccadic interval, suggesting enhanced global network integrate information across separate cortical modules.

Furthermore, our results showed that the energy (*H*) and Shannon entropy (*S*) in the functional brain network are also increased during the presaccadic interval. The *H* value is related to stability of synchronization in the functional brain network (Daianu et al., 2015; Ghaderi et al., 2020, 2021) and *S* is associated with complexity of network (Ghaderi et al., 2019, 2020, 2021). This result suggests that synchronization between functional network nodes (all brain regions) is more stable during the presaccadic interval, which can support fast propagation between cortical nodes. Further, this was accompanied by increased *S* values, suggesting increased complexity of information processing in the brain. This is not a trivial observation: in some functional brain networks *H* and *S* show inverse correlations (Ghaderi et al. 2020). Since the value of *S* in a complex network is related to diversity of functional weights, the increased *S* in the presaccadic interval shows the brain uses more diverse neural pathways for information processing in the presaccadic interval.

Since the segregation, integration, synchronization, and complexity of brain network were simultaneously and specifically enhanced during the presaccadic interval (compared to fixation), one can justify the existence of a *presaccadic* network. This highly efficient and synchronized network could provide a neural basis for the rapid integration of pre- and post- saccadic visual information during the saccade. Conversely, recent evidence suggests that time, space and movement perception are closely related to states of transient neural network, then the *presaccadic* network can be an appropriate candidate to explain various perisaccadic distortions in time, space and movement (Burr et al., 2011; Eagleman, 2005). For example, the features of the *presaccadic* network can be associated with saccadic *remapping* that needs very fast information processing on the local level and rapid integration between different brain areas on the global level (Morrone et al., 2005). This suggests that the presaccadic network should interact with presaccadic visual signals, as we consider next.

4-3: Stimulus repetition alters the presaccadic cortical network.

We employed presaccadic stimulus repetition as a means to probe signal interactions between visual processing and saccades at both local and network levels. Previous psychophysical studies have indicated that stimulus repetition influences perception of a

subsequently presented novel stimulus (Grill-Spector et al., 2006; Matthews & Gheorghiu, 2016), but here it yielded only modest main EEG effects in our combined saccade-fixation dataset. However, stimulus repetition yielded significant interactions with fixation vs. saccades. This interaction was accompanied by an alteration in both current density (local activation) and centrality (network connectivity) in precuneus, again consistent with a role for this structure precuneus in complex task-related visual processing in the presaccadic interval (Dyckman et al., 2007; Mort et al., 2003; Simon et al., 2002). Further, this interaction affected the centrality of dorsolateral prefrontal cortex. Lateral prefrontal cortex is involved in executive control for saccade tasks (Koval et al., 2011; Ploner et al., 2005) and increased attention to a novel visual stimulus (Heeman et al., 2014). Lastly, SMG centrality was altered by saccade-repetition interactions, consistent with recent fMRI studies that showed a specific sensitivity of SMG to stimulus orientation changes (similar to those here) in the presence of saccades (Dunkley et al., 2016; Baltaretu et al. 2020)

When we performed a post-hoc analysis on fixation and saccades separately, stimulus repetition had no significant effect in our EEG blocks of fixation data. This is consistent with previous EEG/MEG studies showing no significant effects of repetition over short time scales (<100ms) after novel stimulus onset (Cycowicz & Friedman, 2007; Friedman, Cycowicz, & Gaeta, 2001). However, when a repeated series of stimulus was presented before the saccade (saccade/repetition condition), the regional current density and network features in the perisaccadic interval were significantly influenced by stimulus repetition. In lower frequencies (i.e., theta and alpha bands), presaccadic stimulus repetition decreased current density in frontal and parietal cortex, whereas in the beta band current density increased in the central areas, and in the gamma band, current density is increased in posterior regions while decreasing in the frontal cortex.

Furthermore, right superior parietal lobe / precuneus (theta band), right inferior parietal lobe (alpha band), and V1 / dorsolateral prefrontal cortex (gamma band) exhibited higher Eig_C when a pre-saccadic stimulus was repeatedly presented before saccade, signifying more involvement in a functional network (Fig. 10). On the other hand, SMG (gamma band) exhibited decreased Eig_C during presaccadic repetition perhaps

consistent with repetition suppression seen in SMG during fMRI studies signals (Baltaretu et al., 2020; Dunkley et al., 2016). This area may be a human extension of the lateral intraparietal cortex in the monkey (Subramanian & Colby, 2014) and plays a role in trans-saccadic integration of visual signals (Baltaretu et al., 2020; Dunkley et al., 2016). These various hubs, in turn, showed widespread connectivity throughout occipital, temporal, parietal, and frontal cortex, indicating extensive saccade-dependent sharing of visual signals throughout the brain.

Overall, our GTA results showed that the pre-saccadic repetition reduced the entropy of presaccadic network in the theta, beta, and gamma bands. However, clustering coefficient and global efficiency was increased after pre-saccadic repetition. This decreased complexity and increased integration and segregation with same level of synchronizability (for the same energy), suggests the level of information processing was reduced in the presaccadic interval when a pre-saccadic stimulus was presented repeatedly before the saccade. However, this processing was occurring in a more topologically efficient network (with higher integration and segregation). Based on this, one can say that presaccadic stimulus repetition facilitates information processing in the presaccadic network. More generally, this suggests that in the presaccadic interval, visual processing networks are extensively influenced throughout the brain. These altered network properties may also be associated with perisaccadic changes in space and/or time perception (Burr et al., 2011; Eagleman, 2005; Morrone et al., 2005).

5- Conclusion

The results of this study reveal new aspects of neural mechanisms in the presaccadic interval. First, the use of high-density EEG in combination with source localization largely confirms the regional cortical specificity for saccades and presaccadic stimulus repetition observed in fMRI studies, but over more specific time scales (and broader accessibility than MEG). More importantly, the application of Graph Theory Analysis provided objective identification of hubs and functional networks for these processes within a relatively large-scale presaccadic network. Finally, topological analysis of this presaccadic network showed increased levels of integration, segregation, synchronizability and complexity, indicating an accelerated rate and scale of cortical

information processing just before saccades. Overall, this study identifies a *presaccadic network* with major hubs in parieto-frontal cortex, but with connectivity and interactions / influence on visual processing throughout the cerebral cortex. It is likely that this approach will prove useful in explaining the various perceptual distortions that occur in the presaccadic interval.

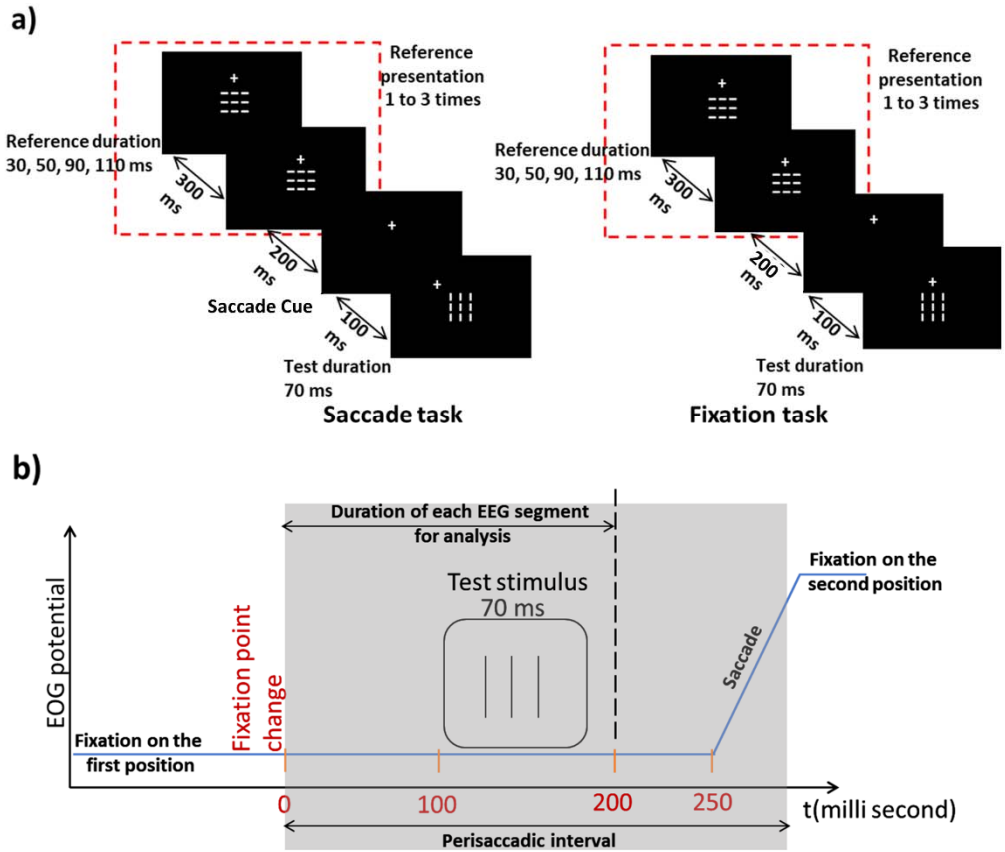

Figure 1: Task configurations. a) the reference stimulus (with varied duration) was presented 1 to 3 times, then the test stimulus (with fixed duration) was shown. The orientation of the reference and test stimulus were always opposite. The interstimulus interval was 300 ms. In the *saccade* task, participants were cued to perform a saccade 100 ms before the presentation of the *test* stimulus. The *fixation task* was the same overall, but participants continued fixating after stimulus presentation. b) A schematic representation of the timing of events and EEG analysis in the saccade task. EEG signals were analyzed for 200 ms across the test stimulus period, which fell in the presaccadic interval of the saccade task (or equivalent period for fixation task).

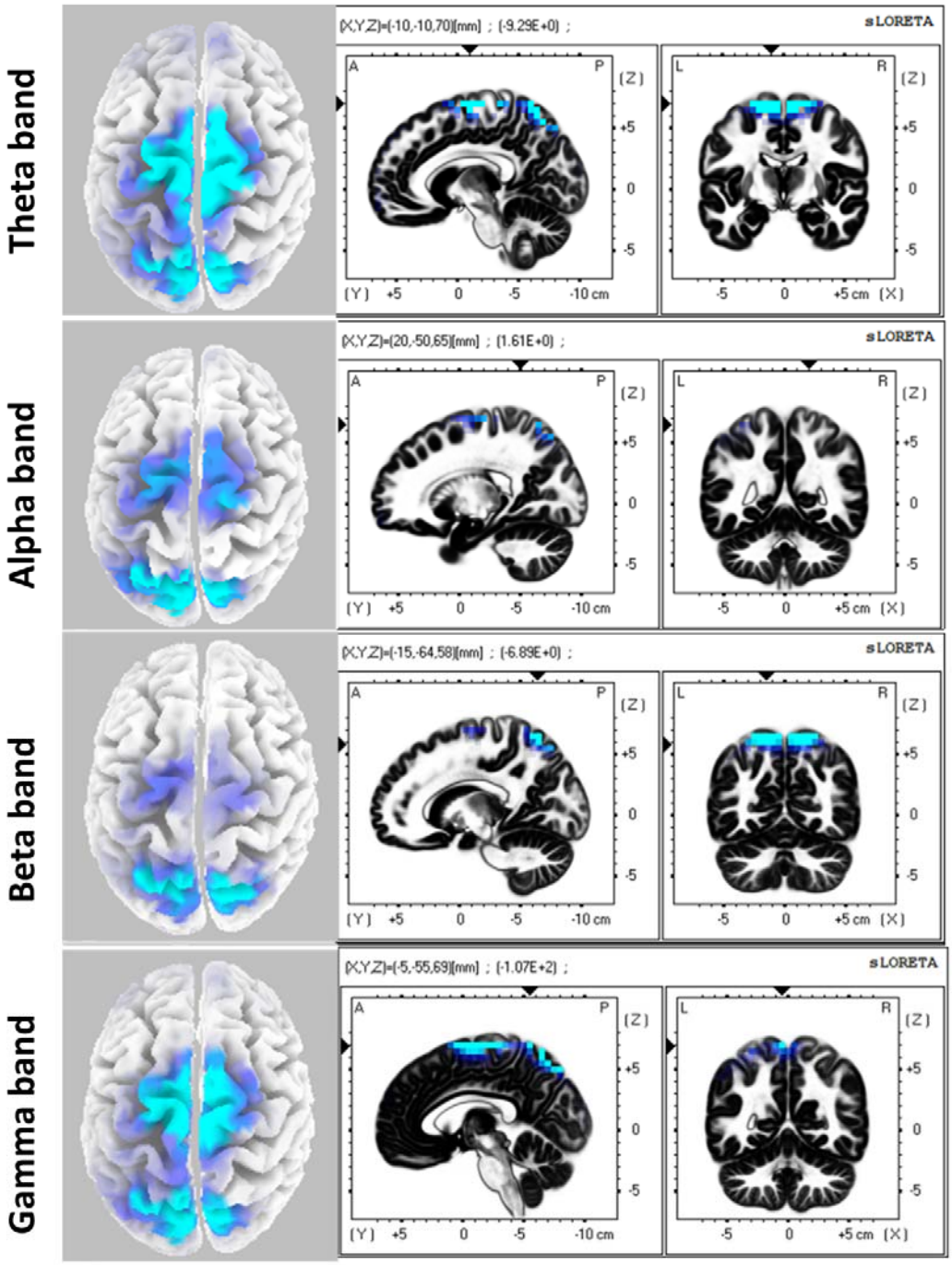

Figure 2: Significant EEG current density differences between the saccade condition and fixation condition for each frequency band (rows). Source localized EEG are projected (by sLORETA) onto a 3D model of the cortical surface from the above view (left column) as well as onto anatomic scans (according to sLORETA map) from the

sagittal and coronal views (right columns). The blue color shows decreased current density in the *saccade* condition in comparison to the *fixation* condition. The scale of colors from dark to light blue *t-value*s from a two-tailed permutation *t-test* (lighter color shows higher *t-values*). The *t-value*s below the threshold of significant level have not been shown.

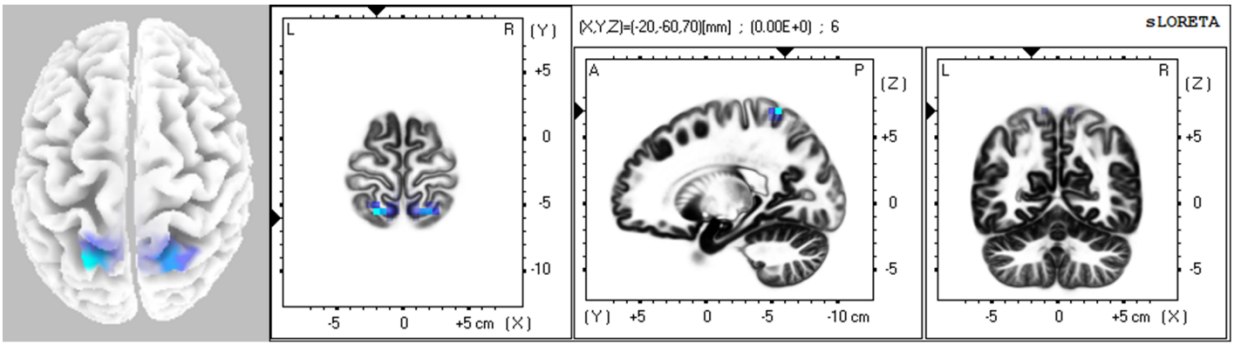

Figure 3: Significant EEG current density differences between the *repetition* condition and *no-repetition* for ??? band. Source localized EEG are projected (by sLORETA) onto a 3D model of the cortical surface from the above view (left column) as well as onto anatomic scans (according to sLORETA map) from the sagittal and coronal views (right columns). condition. The blue color shows decreased current density in the *repetition* condition in comparison to the *no-repetition* condition. The spectrum of colors from light blue to dark blue is related to *t-value*s in two tails permutation *t-test* (lighter color shows higher *t-values*). The *t-value*s below the threshold of significant level has not been shown.

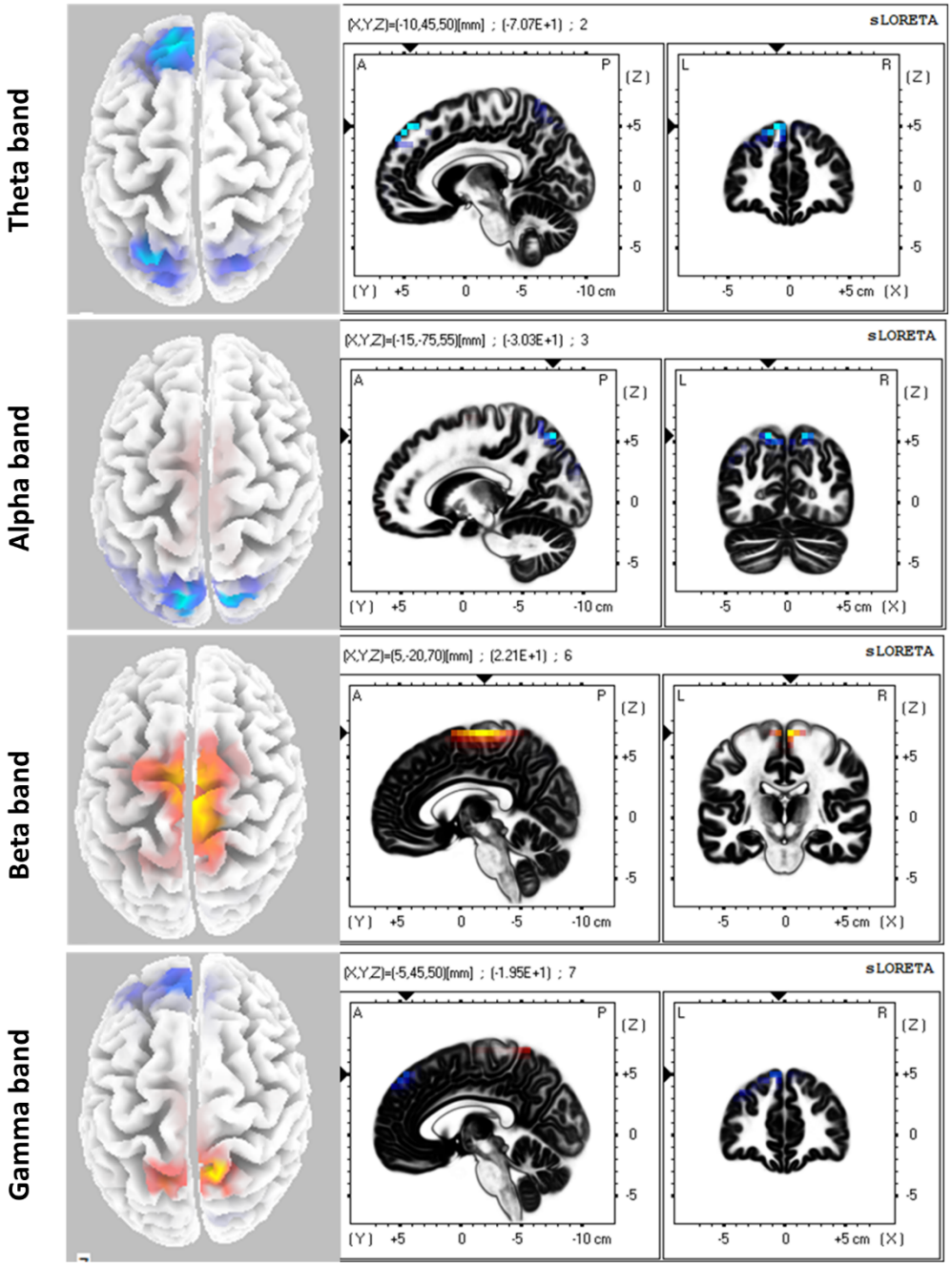

Figure 4: Significant EEG current density differences between the *saccade* condition and the *saccade/repetition* condition for each frequency band (rows). Source localized EEG are projected (by sLORETA) onto a 3D model of the cortical surface from the above view (left column) as well as onto anatomic scans (according to sLORETA map) from the sagittal and coronal views (right columns).

The blue regions are related to decreased current density and the red and yellow regions are related to increased current density in the *saccade/repetition* condition in comparison to the *saccade* condition. The spectrum of colors from light blue to yellow is related to *t-value*s in two tails permutation *t-test* (lighter colors shows higher *t-values*). The *t-value*s below significant threshold has not been shown.

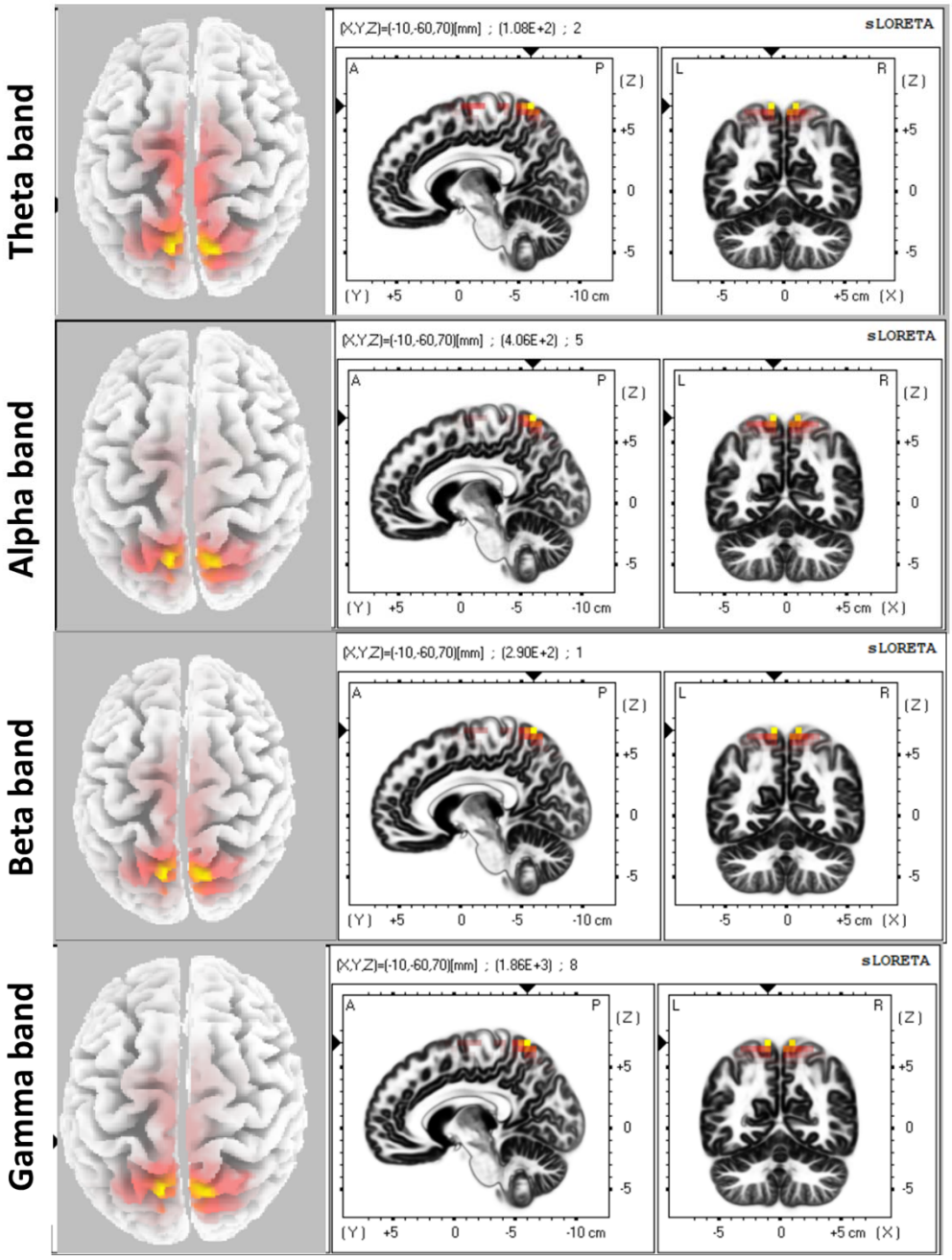

Figure 5: Significant EEG current density differences between SR-S and FR-F for each frequency band (rows). Source localized EEG are projected (by sLORETA) onto a 3D model of the cortical surface from the above view (left column) as well as onto anatomic scans (according to sLORETA map) from the sagittal and coronal views (right columns). The red to yellow regions are related to increased current density in the *SR-S* in comparison to the *FR-F*. The spectrum of colors from red to yellow is related to *t-value*s

in two tails permutation *t-test* (yellow color shows higher *t-values* that are higher than significant threshold.

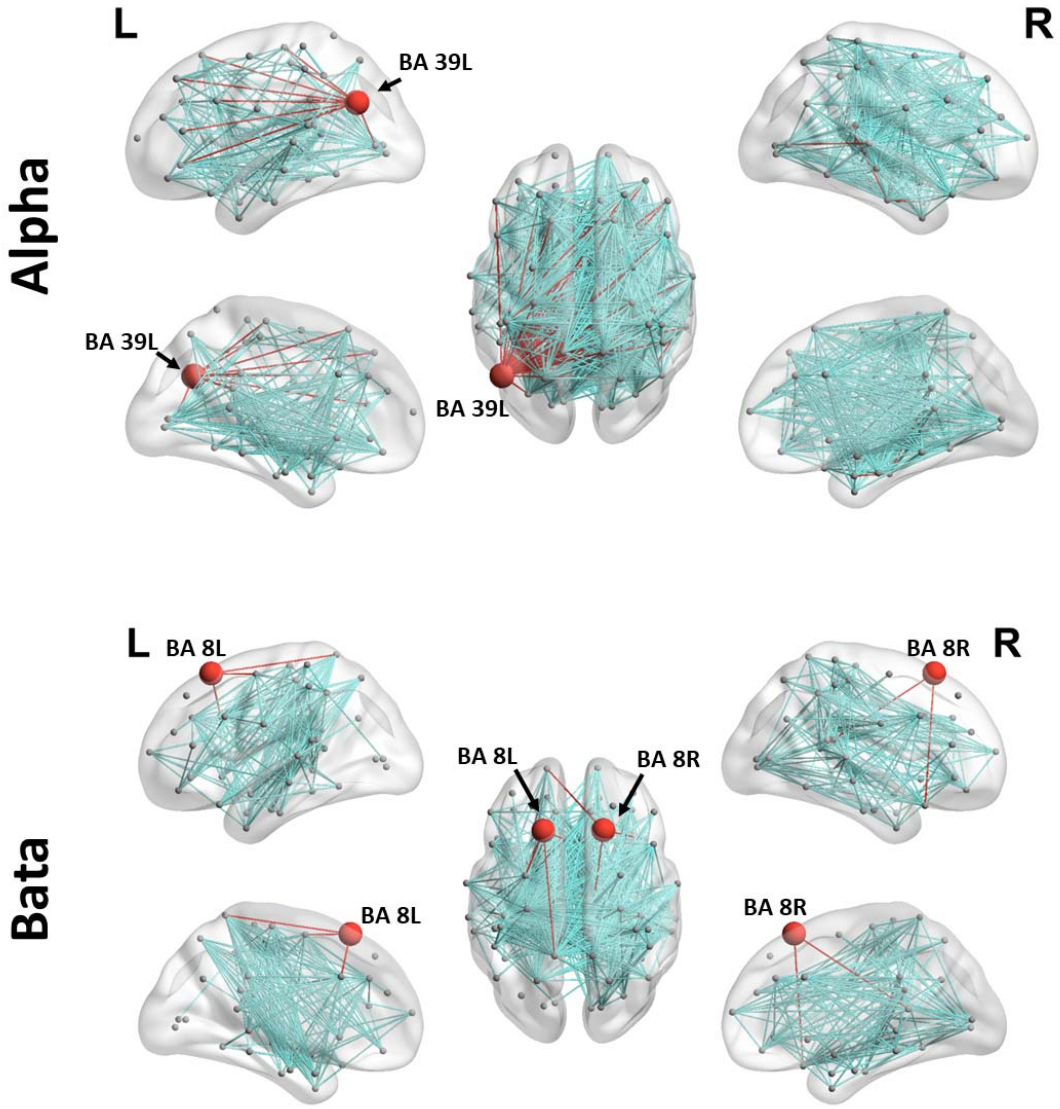

Figure 6: GTA connectivity maps in the *saccade* condition vs. *fixation* condition comparison. Data are projected onto lateral (upper row), upper (middle) and medial (lower row) views of the left (L) and right (R) representations of cortex (generated by BrainNet Viewer toolbox(Xia, Wang, & He, 2013), MALTAB R2019). Brodmann areas that showed significant differences of centrality between conditions were considered as

hubs and are shown by bolded red dots, and their connections are highlighted in red. The 20% of strongest connections related to differences between conditions (*saccade-fixation*) are shown as connectivity lines (edges), in blue-green for non-hub connections.

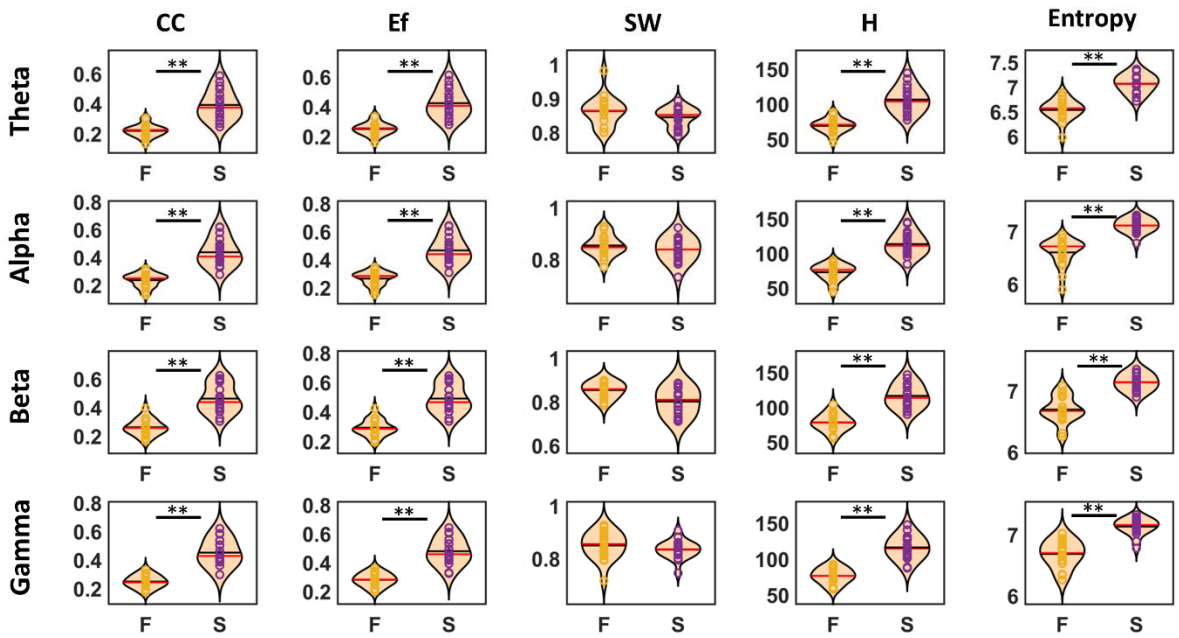

Figure 7: The violin bar plots of network indices in the *fixation* and the *saccade* conditions. Each dot present one individual and the width/shape of violin plots shows distributions of measures for all individuals (Violin plots combine the attributes of standard bar graphs and standard frequency histograms but arranged vertically with frequency shown bidirectionally in the horizontal dimension). The * indicates $p<0.05$ and the ** indicates $p<0.005$. F: fixation condition, S: saccade condition, CC: clustering coefficient, Ef: global efficiency, SW: smallworldness, and H: energy.

Statistical details: *Clustering coefficient* (theta: $t=7.18$, $p<0.001$; alpha: $t=8.78$, $p<0.001$; beta: $t=7.67$, $p<0.001$; gamma: $t=8.14$, $p<0.001$), *global efficiency* (theta: $t=7.38$, $p<0.001$; alpha: $t=9.04$, $p<0.001$; beta: $t=7.82$, $p<0.001$; gamma: $t=8.17$, $p<0.001$), *energy* (theta: $t=8.85$, $p<0.001$; alpha: $t=10.84$, $p<0.001$; beta: $t=9.32$, $p<0.001$; gamma: $t=9.36$, $p<0.001$), and *entropy* (theta: $t=10.31$, $p<0.001$; alpha: $t=9.34$, $p<0.001$; beta: $t=8.58$, $p<0.001$; gamma: $t=8.60$, $p<0.001$).

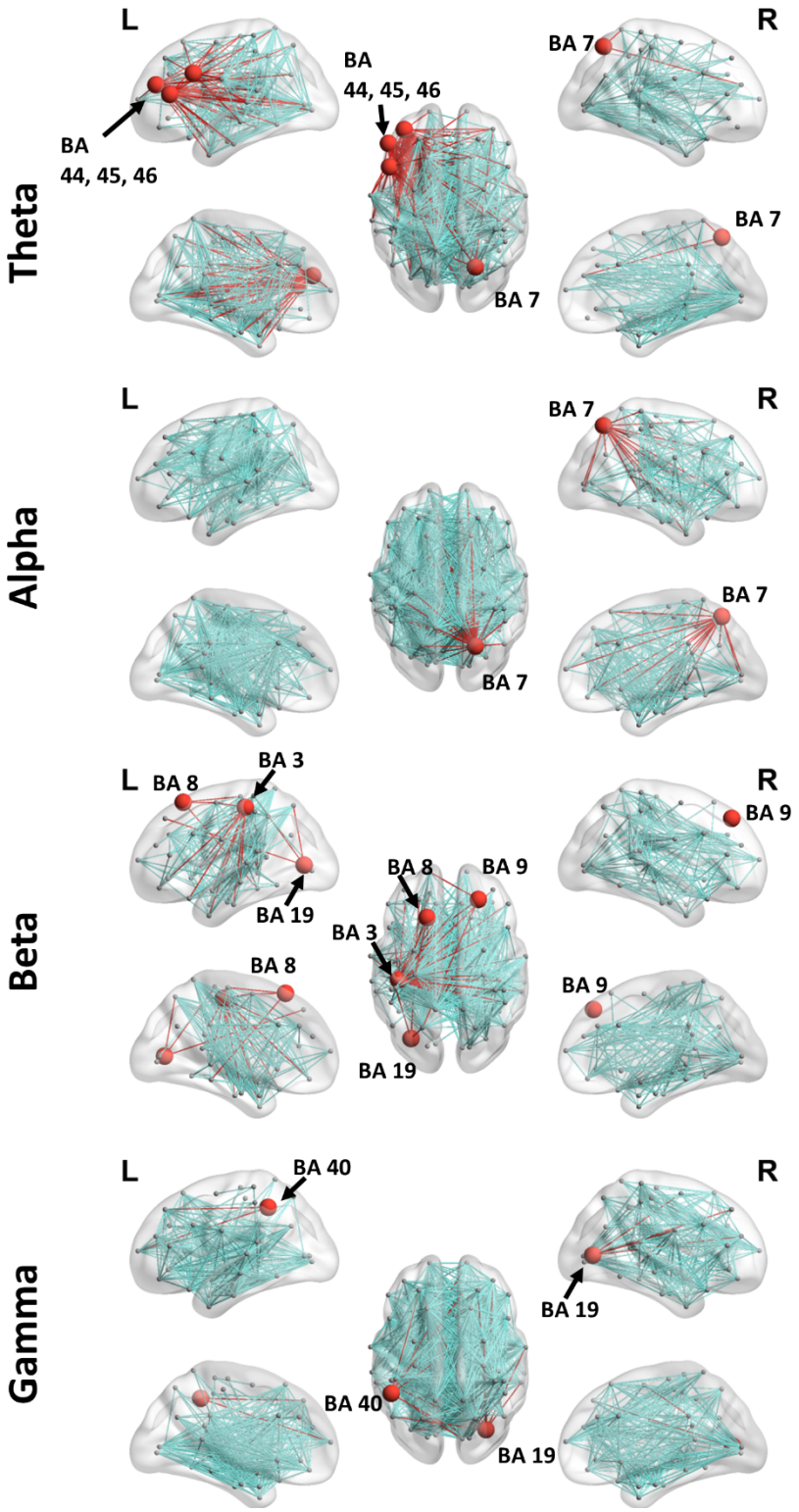

Figure 8: GTA connectivity maps in the *saccade* condition vs. *fixation* condition comparison. Data are projected onto lateral (upper row), upper (middle) and medial (lower row) views of the left (L) and right (R) representations of cortex (generated by

BrainNet Viewer toolbox(Xia et al., 2013), MALTAB R2019). Brodmann areas that showed significant differences of centrality between conditions were considered as hubs and are shown by bolded red dots, and their connections are highlighted in red. The 20% of strongest connections related to differences between conditions (*saccade-fixation*) are shown as connectivity lines (edges), in blue-green for non-hub connections.

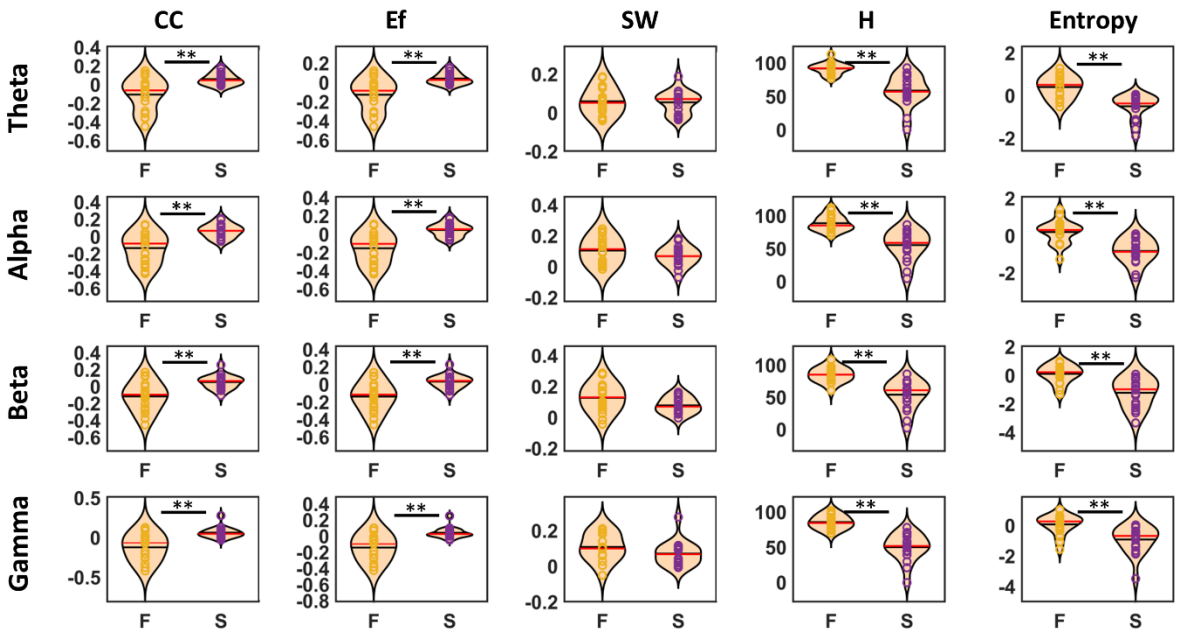

Figure 9: The violin bar plots of network indices in the *fixation* and the *saccade* conditions. Each dot present one individual and the width/shape of violin plots shows distributions of measures for all individuals (Violin plots combine the attributes of standard bar graphs and standard frequency histograms but arranged vertically with frequency shown bidirectionally in the horizontal dimension). The * indicates p<0.05 and the ** indicates p<0.005. F: fixation condition, S: saccade condition, CC: clustering coefficient, Ef: global efficiency, SW: smallworldness, and H: energy.

Statistical details: *Clustering* coefficient (theta: t= 3.59 , p= 0.002; alpha: t= 4.92 , p<0.001 ; beta: t= 4.18 , p<0.001 ; gamma: t= 4.62 , p<0.001), *global efficiency* (theta: t=3.85 , p=0.001 ; alpha: t= 5.23 , p<0.001 ; beta: t= 4.43, p<0.001; gamma: t= 4.79, p<0.001), *energy* (theta: t= 6.20, p<0.001; alpha: t= 5.47 , p<0.001 ; beta: t= 5.10 , p<0.001 ; gamma: t= 8.05 , p<0.001), *entropy* (theta: t= 4.33 , p= p<0.001 ; alpha: t= 4.66, p<0.001 ; beta: t= 4.14 , p<0.001 ; gamma: t= 3.99, p<0.001)

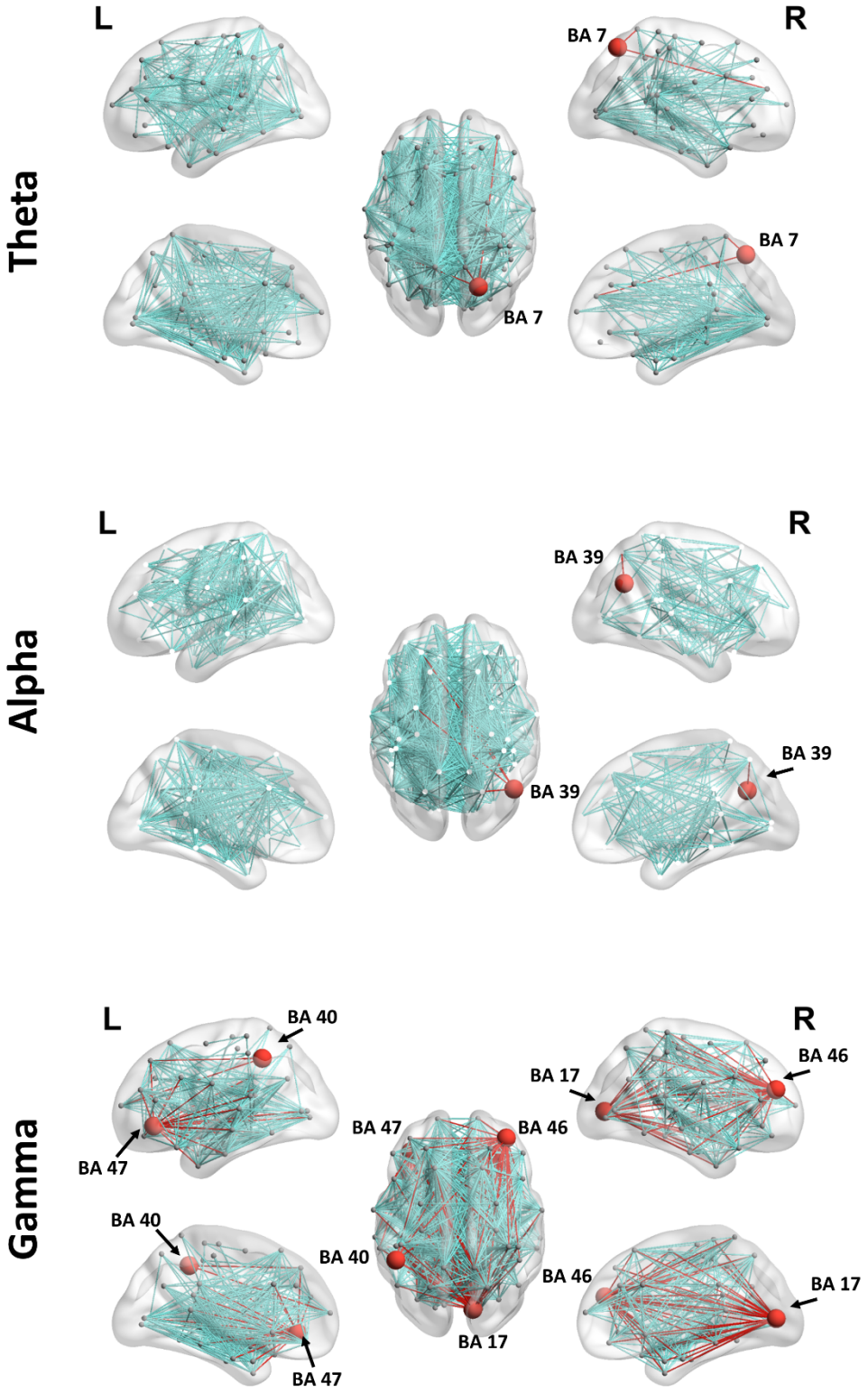
Theta
L
R
BA 7
BA 7
BA 7
Alpha
L
R
BA 39
BA 39
BA 39
Gamma
L
R
BA 40
BA 47
BA 47
BA 40
BA 40
BA 47
BA 46
BA 17
BA 46
BA 46
BA 17
BA 17

Figure 10:

GTA connectivity maps in the *saccade* condition vs. *fixation* condition comparison. Data are projected onto lateral (upper row), upper (middle) and medial (lower row) views of the left (L) and right (R) representations of cortex (generated by BrainNet Viewer toolbox(Xia et al., 2013), MALTAB R2019). Brodmann areas that showed significant differences of centrality between conditions were considered as hubs and are shown by bolded red dots, and their connections are highlighted in red. The 20% of strongest connections related to differences between conditions (*saccade-fixation*) are shown as connectivity lines (edges), in blue-green for non-hub connections.

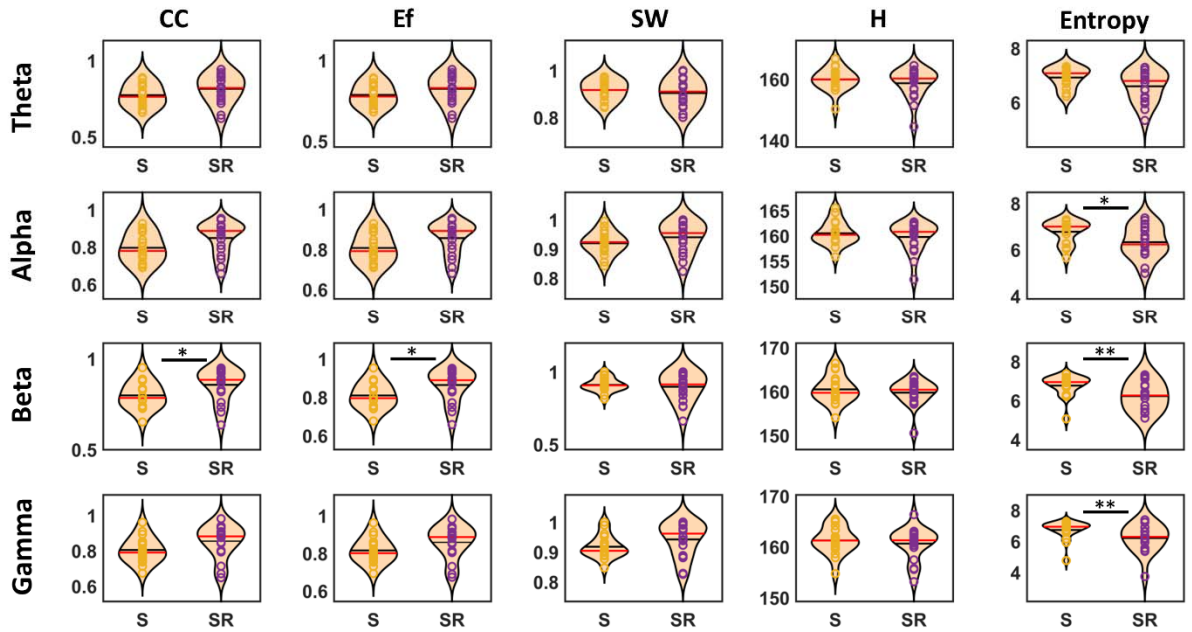

Figure 11: The violin bar plots of network indices in the *fixation* and the *saccade* conditions. Each dot present one individual and the width/shape of violin plots shows distributions of measures for all individuals (Violin plots combine the attributes of standard bar graphs and standard frequency histograms but arranged vertically with frequency shown bidirectionally in the horizontal dimension). The * indicates $p<0.05$ and the ** indicates $p<0.005$. F: fixation condition, S: saccade condition, CC: clustering coefficient, Ef: global efficiency, SW: small-worldness, and H: energy.

Table1: Description of graph theory indices in this study

Index type	Index (Abbreviation)	Equation	Description
Topological indices	*Clustering coefficient (CC)*	$C_i^{wei,0} = \frac{1}{d_i(d_i-1)} \sum_{\substack{1 \le j,l \le N \\ j,l \ne i}} \frac{(w_{ij} w_{il} w_{lj})^{1/3}}{max \quad w_{i,j,l}}$ d_i:: The *degree* of the node *'i'* w_{ij}: : The connectivity weight between the nodes *'i'* and *'j'* $max \quad w_{i,j,l}$: maximum weight between nodes in triangle (Saramäki et al., 2007).	In a weighted network, *CC* is related to strength of connections (weights) among all triangles (three nodes that are connected to each other). Higher weights among triangles increase value of *CC*. If all three connections in triangles are maximum, then *C=1* (the maximum value). In a functional brain network, segregation and local information processing are related to the average of *CC* over all nodes.
	Global efficiency (Ef)	$Ef = \frac{1}{n(n-1)} \sum_{i,j \in N} (L_{ij})^{-1}$ L_{ij}: Shortest path length (strongest connection) between nodes *i* and *j* n: (network size) number of nodes N: N*atural* numbers (Rubinov & Sporns, 2010)	In a weighted network, the *Ef* is inversely associated with the shortest path between nodes. The *Ef* exhibits the level of integration in the network.
	Eigenvector centrality (Eig_C)	$Ax = Eig_L x$ $x = [Eig_{Cent1}, Eig_{Cent2}, \ldots, Eig_{Cent19}]$ A: Adjacency matrix Eig_L: The largest eigenvalue x: Eigenvector that is corresponded to the largest eigenvalue. It contains 19 arrays (equal to the number of nodes) (Ghaderi et al., 2020)	In a weighted network, the Eig_{Cent} of nodes is the eigenvector set related to the largest eigenvalue of the adjacency matrix. Each array in this vector is the Eig_{Cent} of each node (in the order of node presentation in the adjacency matrix).
Dynamical index	*Energy (H)*	$H = \sum_{i=1}^{n} \lvert \lambda_i \rvert$ λ_i: Eigenvalues of graph n: Number of nodes (Ghaderi et al., 2020)	In an undirected, symmetric, and weighted network, *H* equals to the summation of eigenvalues (absolute values) and is associated with stability of synchronization in the network.
Complexity index	*Shannon entropy (S)*	$S = -\sum_i p_i \, log_2 \, p_i$ p_i: The probability of occurrence of *'i'* (Shannon & warren weaver, 1949)	In a weighted network, the *S* is calculated by considering the probability of occurrence of all weights in the adjacency matrix. The minimum *S* is achieved when all the weights are same. *S* is maximal when weights in adjacency matrix are nonrepetitive.

Table 2: Brodmann areas and corresponded anatomical regions

Brodmann area	Anatomical region	Talairach coordinates (X, Y, Z)
BA 3	BA 3 is in the postcentral gyrus and contains some regions of primary somatosensory cortex (Strotzer, 2009).	(46, -19, 52)
BA 5, 7	In human cortex, BA 5 and 7 are associated with posterior parietal regions. BA 5 contains superior parietal lobule and BA 7 contains precuneus and parts of superior parietal lobule (Garey, 1999).	BA 5: (11, -43, 60) BA 7: (11, -66, 63)
BA 8	In the human cortex, BA 8 is a part of frontal cortex and contains frontal eye field region (Paus, 1996).	(12, 27, 53)
BA 9	In the human cortex, BA 9 is in frontal cortex and is associated with dorsolateral and medial prefrontal cortex (Rajkowska & Goldman-Rakic, 1995).	(14, 46, 37)
BA 40	BA 40 is a part of parietal cortex and contains inferior lateral regions of parietal cortex and especially supramarginal gyrus (Rushworth, Behrens, & Johansen-Berg, 2006).	(41, -39, 52)
BA 44, 45	In the human cortex, BA 44, 45 are parts of frontal cortex and contain regions of inferior frontal gyrus (Garey, 1999).	BA 44: (52, 13, 15) BA 45: (-38, 21, 6)
BA 46	In the human cortex, BA 46 is in frontal cortex and contains the regions of dorsolateral prefrontal cortex (Rajkowska & Goldman-Rakic, 1995).	(-33, 30, 12)

Table 3: The statistical details of comparisons between *saccade* and *fixation* conditions.

	Frequency band	**Significance level**	**Regions with significant differences after FDR analysis**
Saccade* vs. *Fixation	**Theta**	Two-Tailed (A<>B): t(0.05)=4.321, p=0.01040	In the saccade condition, current density was bilaterally suppressed in superior / medial frontal, precuneus and superior parietal regions.
	Alpha	Two-Tailed (A<>B): t(0.05)=5.540, p=0.00020	In the saccade condition, current density was bilaterally suppressed in superior frontal, precuneus and superior parietal regions.
	Beta	Two-Tailed (A<>B): t(0.05)=4.535, p=0.01340	In the saccade condition, current density was bilaterally suppressed in superior frontal, precuneus and superior parietal regions.
	Gamma	Two-Tailed (A<>B): t(0.05)=4.405, p=0.00020	In the saccade condition, current density was bilaterally suppressed in superior / medial frontal, precuneus and superior parietal regions.
Saccade* vs. *Saccade/repetition	**Theta**	Two-Tailed (A<>B): t(0.05)=4.321, p=0.01040	In the saccade/repetition condition, current density was suppressed in the superior frontal gyrus (left side) and in precuneus (both sides).
	Alpha	Two-Tailed (A<>B): t(0.05)=4.321, p=0.01040	In the saccade/repetition condition, current density was suppressed in precuneus (both sides).
	Beta	Two-Tailed (A<>B): t(0.05)=5.540, p=0.00020	In the saccade/repetition condition current density was bilaterally enhanced in the medial frontal and post central gyrus.
	Gamma	Two-Tailed (A<>B):	In the saccade/repetition condition

		t(0.05)=4.535, p=0.01340	current density was decreased in the superior frontal gyrus (left side) and enhanced in the superior parietal lobe (both sides).
Interactions: (SR-S)-(FR-F)	**Theta**	Two-Tailed (A<>B): t(0.05)=3.721, p=0.01770	The activity of *SR-S* was significantly higher than *FR-F* in bilateral precuneus region
	Alpha	Two-Tailed (A<>B): t(0.05)=4.321, p=0.01040	
	Beta	Two-Tailed (A<>B): t(0.05)=4.535, p=0.01340	
	Gamma	Two-Tailed (A<>B): t(0.05)=4.321, p=0.01040	

Alkan, Y., Biswal, B. B., Taylor, P. A., & Alvarez, T. L. (2011). Segregation of frontoparietal and cerebellar components within saccade and vergence networks using hierarchical independent component analysis of fMRI. *Visual Neuroscience*, *28*(3), 247–261. https://doi.org/10.1017/S0952523811000125

Andersen, R. A., Asanuma, C., Essick, G., & Siegel, R. M. (1990). Corticocortical connections of anatomically and physiologically defined subdivisions within the inferior parietal lobule. *Journal of Comparative Neurology*, *296*(1), 65–113. https://doi.org/https://doi.org/10.1002/cne.902960106

Anderson, T. J., Jenkins, I. H., Brooks, D. J., Hawken, M. B., Frackowiak, R. S. J., & Kennard, C. (1994). Cortical control of saccades and fixation in man A PET study. *Brain*, *117*(5), 1073–1084. https://doi.org/10.1093/brain/117.5.1073

Asadzadeh, S., Yousefi Rezaii, T., Beheshti, S., Delpak, A., & Meshgini, S. (2020). A

systematic review of EEG source localization techniques and their applications on diagnosis of brain abnormalities. *Journal of Neuroscience Methods*. https://doi.org/10.1016/j.jneumeth.2020.108740

Atay, F. M., Biyiko□lu, T., & Jost, J. (2006). Network synchronization: Spectral versus statistical properties. *Physica D: Nonlinear Phenomena*. https://doi.org/10.1016/j.physd.2006.09.018

Bahill, A. T., Clark, M. R., & Stark, L. (1975). Dynamic overshoot in saccadic eye movements is caused by neurological control signal reversals. *Experimental Neurology*, *48*(1), 107–122. https://doi.org/https://doi.org/10.1016/0014-4886(75)90226-5

Baltaretu, B. R., Monaco, S., Velji-Ibrahim, J., Luabeya, G. N., & Douglas Crawford, J. (2020). Parietal cortex integrates saccade and object orientation signals to update grasp plans. *Journal of Neuroscience*. https://doi.org/10.1523/JNEUROSCI.0300-20.2020

Barash, S., Bracewell, R. M., Fogassi, L., Gnadt, J. W., & Andersen, R. A. (1991). Saccade-related activity in the lateral intraparietal area. II. Spatial properties. *Journal of Neurophysiology*, *66*(3), 1109–1124. https://doi.org/10.1152/jn.1991.66.3.1109

Bassett, D. S.□;, & Bullmore, E. T. (2007). Small-World Brain Networks Danielle. *Indian Journal of Environmental Protection*. https://doi.org/10.1177/1073858406293182

Bassett, Danielle S, & Sporns, O. (2017). Network neuroscience. *Nature Neuroscience*. https://doi.org/10.1038/nn.4502

Bassett, Danielle Smith, & Bullmore, E. (2006). Small-world brain networks. *Neuroscientist*. https://doi.org/10.1177/1073858406293182

Bell, A. H., Meredith, M. A., Van Opstal, A. J., & Munoz, D. P. (2005). Crossmodal integration in the primate superior colliculus underlying the preparation and initiation of saccadic eye movements. *Journal of Neurophysiology*, *93*(6), 3659–3673. https://doi.org/10.1152/jn.01214.2004

Berman, R. A., Colby, C. L., Genovese, C. R., Voyvodic, J. T., Luna, B., Thulborn, K. R., & Sweeney, J. A. (1999). Cortical networks subserving pursuit and saccadic eye movements in humans: An FMRI study. *Human Brain Mapping*, *8*(4), 209–225. https://doi.org/https://doi.org/10.1002/(SICI)1097-0193(1999)8:4<209::AID-HBM5>3.0.CO;2-0

Bialonski, S., & Lehnertz, K. (2013). Assortative mixing in functional brain networks during epileptic seizures. *Chaos*. https://doi.org/10.1063/1.4821915

Binda, P., Cicchini, G. M., Burr, D. C., & Morrone, M. C. (2009). Spatiotemporal Distortions of Visual Perception at the Time of Saccades. *Journal of Neuroscience*, *29*(42), 13147–13157. https://doi.org/10.1523/JNEUROSCI.3723-09.2009

Blohm, G., Alikhanian, H., Gaetz, W., Goltz, H. C., DeSouza, J. F. X., Cheyne, D. O., & Crawford, J. D. (2019). Neuromagnetic signatures of the spatiotemporal transformation for manual pointing. *NeuroImage*, *197*, 306–319. https://doi.org/https://doi.org/10.1016/j.neuroimage.2019.04.074

Boccaletti, S., Latora, V., Moreno, Y., Chavez, M., & Hwang, D. U. (2006). Complex networks: Structure and dynamics. *Physics Reports*. https://doi.org/10.1016/j.physrep.2005.10.009

Bremmer, F., Kubischik, M., Hoffmann, K. P., & Krekelberg, B. (2009). Neural dynamics of saccadic suppression. *Journal of Neuroscience*. https://doi.org/10.1523/JNEUROSCI.2908-09.2009

Brignani, D., Maioli, C., Maria Rossini, P., & Miniussi, C. (2007). Event-related power modulations of brain activity preceding visually guided saccades. *Brain Research*. https://doi.org/10.1016/j.brainres.2006.12.018

Buchholz, V. N., Jensen, O., & Medendorp, W. P. (2014). Different roles of alpha and beta band oscillations in anticipatory sensorimotor gating. *Frontiers in Human Neuroscience*, Vol. 8. https://doi.org/10.3389/fnhum.2014.00446

Bullmore, E., & Sporns, O. (2009). Complex brain networks: graph theoretical analysis of structural and functional systems. *Nature Reviews. Neuroscience*.

https://doi.org/10.1038/nrn2575

Bullmore, E., & Sporns, O. (2012). The economy of brain network organization. *Nature Reviews Neuroscience*, *13*(5), 336–349. https://doi.org/10.1038/nrn3214

Burr, D. C., & Morrone, M. C. (2011). Spatiotopic coding and remapping in humans. *Philosophical Transactions of the Royal Society B: Biological Sciences*, *366*(1564), 504–515. https://doi.org/10.1098/rstb.2010.0244

Burr, D. C., Morrone, M. C., & Ross, J. (1994). Selective suppression of the magnocellular visual pathway during saccadic eye movements. *Nature*, *371*(6497), 511–513. https://doi.org/10.1038/371511a0

Burr, D. C., Ross, J., Binda, P., & Morrone, M. C. (2011). Saccades Compress Space, Time, and Number. *Space, Time and Number in the Brain*, *14*(12), 175–186. https://doi.org/10.1016/B978-0-12-385948-8.00012-8

Busch, N. A., Dubois, J., & VanRullen, R. (2009). The phase of ongoing EEG oscillations predicts visual perception. *Journal of Neuroscience*. https://doi.org/10.1523/JNEUROSCI.0113-09.2009

Chen, Y., & Crawford, J. D. (2017). Cortical activation during landmark-centered vs. Gaze-centered memory of saccade targets in the human: An FMRI study. *Frontiers in Systems Neuroscience*. https://doi.org/10.3389/fnsys.2017.00044

Chen, Y., Monaco, S., & Crawford, J. D. (2018). Neural substrates for allocentric-to-egocentric conversion of remembered reach targets in humans. *European Journal of Neuroscience*. https://doi.org/10.1111/ejn.13885

Corbetta, M., Akbudak, E., Conturo, T. E., Snyder, A. Z., Ollinger, J. M., Drury, H. A., … Shulman, G. L. (1998). A Common Network of Functional Areas for Attention and Eye Movements. *Neuron*, *21*(4), 761–773. https://doi.org/https://doi.org/10.1016/S0896-6273(00)80593-0

Daianu, M., Mezher, A., Jahanshad, N., Hibar, D. P., Nir, T. M., Jack, C. R., … Thompson, P. M. (2015). Spectral graph theory and graph energy metrics show evidence for the Alzheimer's disease disconnection syndrome in APOE-4 risk gene

carriers. *Proceedings - International Symposium on Biomedical Imaging*, *2015-July*, 458–461. https://doi.org/10.1109/ISBI.2015.7163910

Deco, G., Tononi, G., Boly, M., & Kringelbach, M. L. (2015). Rethinking segregation and integration: contributions of whole-brain modelling. *Nature Reviews Neuroscience*, *16*(7), 430–439. https://doi.org/10.1038/nrn3963

Duhamel, Colby, C. L., & Goldberg, M. E. (1992). The updating of the representation of visual space in parietal cortex by intended eye movements. *Science*, *255*(5040), 90 LP – 92. https://doi.org/10.1126/science.1553535

Dunkley, B. T., Baltaretu, B., & Crawford, J. D. (2016). Trans-saccadic interactions in human parietal and occipital cortex during the retention and comparison of object orientation. *Cortex*. https://doi.org/10.1016/j.cortex.2016.06.012

Dyckman, K. A., Camchong, J., Clementz, B. A., & McDowell, J. E. (2007). An effect of context on saccade-related behavior and brain activity. *NeuroImage*, *36*(3), 774–784. https://doi.org/https://doi.org/10.1016/j.neuroimage.2007.03.023

Eagleman, D. M. (2005). Distortions of time during rapid eye movements. *Nature Neuroscience*, *8*(7), 850–851. https://doi.org/10.1038/nn0705-850

Fabius, J. H., Fracasso, A., Acunzo, D. J., van der Stigchel, S., & Melcher, D. (2020). Low-level visual information is maintained across saccades, allowing for a postsaccadic handoff between visual areas. *Journal of Neuroscience*. https://doi.org/10.1523/JNEUROSCI.1169-20.2020

Fagerholm, E. D., Hellyer, P. J., Scott, G., Leech, R., & Sharp, D. J. (2015). Disconnection of network hubs and cognitive impairment after traumatic brain injury. *Brain*. https://doi.org/10.1093/brain/awv075

Fairhall, S. L., Schwarzbach, J., Lingnau, A., Van Koningsbruggen, M. G., & Melcher, D. (2017). Spatiotopic updating across saccades revealed by spatially-specific fMRI adaptation. *NeuroImage*, *147*, 339–345. https://doi.org/https://doi.org/10.1016/j.neuroimage.2016.11.071

Forgacs, P. B., Von Gizycki, H., Selesnick, I., Syed, N. A., Ebrahim, K., Avitable, M., …

Bodis-Wollner, I. (2008). Perisaccadic parietal and occipital gamma power in light and in complete darkness. *Perception*. https://doi.org/10.1068/p5875

Frings, L., Wagner, K., Quiske, A., Schwarzwald, R., Spreer, J., Halsband, U., & Schulze-Bonhage, A. (2006). Precuneus is involved in allocentric spatial location encoding and recognition. *Experimental Brain Research*. https://doi.org/10.1007/s00221-006-0408-8

Frost, A., & Niemeier, M. (2015). Suppression and reversal of motion perception around the time of the saccade. *Frontiers in Systems Neuroscience*. https://doi.org/10.3389/fnsys.2015.00143

Funahashi, S., Bruce, C. J., & Goldman-Rakic, P. S. (1991). Neuronal activity related to saccadic eye movements in the monkey's dorsolateral prefrontal cortex. *Journal of Neurophysiology*, *65*(6), 1464–1483. https://doi.org/10.1152/jn.1991.65.6.1464

Garey, L. J. (1999). *Brodmann's' localisation in the cerebral cortex'*. World Scientific.

Ghaderi A.H., Jahan A., Akrami F., S. M. (2021). Transcranial photobiomodulation changes topology, synchronizability, and complexity of resting state brain networks. *Journal of Neural Engineering*. Retrieved from http://iopscience.iop.org/article/10.1088/1741-2552/abf97c

Ghaderi, Amir H., Andevari, M. N., & Sowman, P. F. (2018). Evidence for a Resting State Network Abnormality in Adults Who Stutter. *Frontiers in Integrative Neuroscience*. https://doi.org/10.3389/fnint.2018.00016

Ghaderi, Amir Hossein, Baltaretu, B. R., Andevari, M. N., Bharmauria, V., & Balci, F. (2020). Synchrony and Complexity in State-Related EEG Networks: An Application of Spectral Graph Theory. *Neural Computation*. https://doi.org/10.1162/neco_a_01327

Ghaderi, Amir Hossein, & Crawford, J. D. (2020). Linear vector models of time perception account for saccade and stimulus novelty interactions. *BioRxiv*.

Ghaderi, Amir Hossein, Jahan, A., Akrami, F., & Moghadam Salimi, M. (2021). Transcranial photobiomodulation changes topology, synchronizability, and

complexity of resting state brain networks. *Journal of Neural Engineering*, *18*(4), 46048. https://doi.org/10.1088/1741-2552/abf97c

Ghaderi, Amir Hossein, Moradkhani, S., Haghighatfard, A., Akrami, F., Khayyer, Z., & Balcı, F. (2018). Time estimation and beta segregation: An EEG study and graph theoretical approach. *PLoS ONE*, *13*(4). https://doi.org/10.1371/journal.pone.0195380

Ghaderi, Amir Hossein, Nazari, M. A., & Darooneh, A. H. (2019). Functional brain segregation changes during demanding mathematical task. *International Journal of Neuroscience*, *129*(9), 904–915. https://doi.org/10.1080/00207454.2019.1586688

Ghaderi, Amir Hossein, Nazari, M. A., Shahrokhi, H., & Darooneh, A. H. (2017). Functional brain connectivity differences between different ADHD presentations: Impaired functional segregation in ADHD-combined presentation but not in ADHD-inattentive presentation. *Basic and Clinical Neuroscience*. https://doi.org/10.18869/nirp.bcn.8.4.267

Gitelman, D. R., Nobre, A. C., Parrish, T. B., LaBar, K. S., Kim, Y.-H., Meyer, J. R., & Mesulam, M.-M. (1999). A large-scale distributed network for covert spatial attention: Further anatomical delineation based on stringent behavioural and cognitive controls. *Brain*, *122*(6), 1093–1106. https://doi.org/10.1093/brain/122.6.1093

Grill-Spector, K., Henson, R., & Martin, A. (2006). Repetition and the brain: Neural models of stimulus-specific effects. *Trends in Cognitive Sciences*. https://doi.org/10.1016/j.tics.2005.11.006

Gutman, I. (2013). The Energy of a Graph: Old and New Results. *Algebraic Combinatorics and Applications*, 196–211. https://doi.org/10.1007/978-3-642-59448-9_13

Gutman, I., & Zhou, B. (2006). Laplacian energy of a graph. *Linear Algebra and Its Applications*, *414*(1), 29–37. https://doi.org/10.1016/j.laa.2005.09.008

Hanes, D P, Thompson, K. G., & Schall, J. D. (1995). Relationship of presaccadic

activity in frontal eye field and supplementary eye field to saccade initiation in macaque: Poisson spike train analysis. *Experimental Brain Research*, *103*(1), 85–96. https://doi.org/10.1007/BF00241967

Hanes, Doug P, & Wurtz, R. H. (2001). Interaction of the Frontal Eye Field and Superior Colliculus for Saccade Generation. *Journal of Neurophysiology*, *85*(2), 804–815. https://doi.org/10.1152/jn.2001.85.2.804

Harris, C. M., & Wolpert, D. M. (2006). The Main Sequence of Saccades Optimizes Speed-accuracy Trade-off. *Biological Cybernetics*, *95*(1), 21–29. https://doi.org/10.1007/s00422-006-0064-x

Hasanzadeh, F., Mohebbi, M., & Rostami, R. (2020). Graph theory analysis of directed functional brain networks in major depressive disorder based on EEG signal. *Journal of Neural Engineering*. https://doi.org/10.1088/1741-2552/ab7613

Heeman, J., Theeuwes, J., & Van der Stigchel, S. (2014). The time course of top-down control on saccade averaging. *Vision Research*. https://doi.org/10.1016/j.visres.2014.03.007

Huddleston, W. E., Swanson, A. N., Lytle, J. R., & Aleksandrowicz, M. S. (2021). Distinct saccade planning and endogenous visuospatial attention maps in parietal cortex: A basis for functional differences in sensory and motor attention. *Cortex*, *137*, 292–304. https://doi.org/https://doi.org/10.1016/j.cortex.2021.01.009

Jerbi, K., Freyermuth, S., Dalal, S., Kahane, P., Bertrand, O., Berthoz, A., & Lachaux, J. P. (2009). Saccade related gamma-band activity in intracerebral EEG: Dissociating neural from ocular muscle activity. *Brain Topography*. https://doi.org/10.1007/s10548-009-0078-5

Jouzizadeh, M., Ghaderi, A. H., Cheraghmakani, H., Baghbanian, S. M., & Khanbabaie, R. (2021). Resting-State Brain Network Deficits in Multiple Sclerosis Participants: Evidence from Electroencephalography and Graph Theoretical Analysis. *Brain Connectivity*. https://doi.org/10.1089/brain.2020.0857

Joyce, K. E., Laurienti, P. J., Burdette, J. H., & Hayasaka, S. (2010). A new measure of

centrality for brain networks. *PLoS ONE*. https://doi.org/10.1371/journal.pone.0012200

Kawasaki, M., & Yamaguchi, Y. (2013). Frontal theta and beta synchronizations for monetary reward increase visual working memory capacity. *Social Cognitive and Affective Neuroscience*. https://doi.org/10.1093/scan/nss027

Keren, A. S., Yuval-Greenberg, S., & Deouell, L. Y. (2010). Saccadic spike potentials in gamma-band EEG: Characterization, detection and suppression. *NeuroImage*. https://doi.org/10.1016/j.neuroimage.2009.10.057

Kern, M., Schulze-Bonhage, A., & Ball, T. (2021). Blink- and saccade-related suppression effects in early visual areas of the human brain: Intracranial EEG investigations during natural viewing conditions. *NeuroImage*, *230*(October 2020), 117788. https://doi.org/10.1016/j.neuroimage.2021.117788

Kitzbichler, M. G., Smith, M. L., Christensen, S. R., & Bullmore, E. (2009). Broadband criticality of human brain network synchronization. *PLoS Computational Biology*. https://doi.org/10.1371/journal.pcbi.1000314

Kleiner, M. (2010). Visual stimulus timing precision in Psychtoolbox-3: Tests, pitfalls and solutions. *33rd European Conference on Visual Perception (ECVP 2010)*, 189. Pion Ltd.

Kleiner, M., Brainard, D., & Pelli, D. (2007). *What's new in Psychtoolbox-3?*

Kleiser, R., Seitz, R. J., & Krekelberg, B. (2004). Neural correlates of saccadic suppression in humans. *Current Biology*. https://doi.org/10.1016/j.cub.2004.02.036

Koval, M. J., Lomber, S. G., & Everling, S. (2011). Prefrontal cortex deactivation in macaques alters activity in the superior colliculus and impairs voluntary control of saccades. *Journal of Neuroscience*. https://doi.org/10.1523/JNEUROSCI.1258-11.2011

Kovalenko, L. Y., & Busch, N. A. (2016). Probing the dynamics of perisaccadic vision with EEG. *Neuropsychologia*. https://doi.org/10.1016/j.neuropsychologia.2015.12.012

Kusunoki, M., & Goldberg, M. E. (2003). The Time Course of Perisaccadic Receptive Field Shifts in the Lateral Intraparietal Area of the Monkey. *Journal of Neurophysiology*, *89*(3), 1519–1527. https://doi.org/10.1152/jn.00519.2002

Larremore, D. B., Shew, W. L., & Restrepo, J. G. (2011). Predicting criticality and dynamic range in complex networks: Effects of topology. *Physical Review Letters*. https://doi.org/10.1103/PhysRevLett.106.058101

Leocani, L., Toro, C., Manganotti, P., Zhuang, P., & Hallett, M. (1997). Event-related coherence and event-related desynchronization/synchronization in the 10 Hz and 20 Hz EEG during self- paced movements. *Electroencephalography and Clinical Neurophysiology - Evoked Potentials*. https://doi.org/10.1016/S0168-5597(96)96051-7

Leoné, F. T. M., Toni, I., & Medendorp, W. P. (2014). Two-dimensional spatial tuning for saccades in human parieto-frontal cortex. *NeuroImage*. https://doi.org/10.1016/j.neuroimage.2013.09.067

Levy, I., Schluppeck, D., Heeger, D. J., & Glimcher, P. W. (2007). Specificity of Human Cortical Areas for Reaches and Saccades. *The Journal of Neuroscience*, *27*(17), 4687 LP – 4696. https://doi.org/10.1523/JNEUROSCI.0459-07.2007

Li, G., Luo, Y., Zhang, Z., Xu, Y., Jiao, W., Jiang, Y., … Wang, C. (2019). Effects of Mental Fatigue on *Small-World* Brain Functional Network Organization. *Neural Plasticity*, *2019*, 1716074. https://doi.org/10.1155/2019/1716074

Li, X., Shi, Y., & Gutman, I. (2012). Graph energy. In *Graph Energy*. https://doi.org/10.1007/978-1-4614-4220-2

Lin, X., Lei, V. L. C., Li, D., Hu, Z., Xiang, Y., & Yuan, Z. (2018). Mapping the small-world properties of brain networks in Chinese to English simultaneous interpreting by using functional near-infrared spectroscopy. *Journal of Innovative Optical Health Sciences*, *11*(03), 1840001. https://doi.org/10.1142/S1793545818400011

Lynall, M.-E., Bassett, D. S., Kerwin, R., McKenna, P. J., Kitzbichler, M., Muller, U., & Bullmore, E. (2013). Functional Connectivity and Brain Networks in Schizophrenia.

Journal of Neuroscience. https://doi.org/10.1523/jneurosci.0333-10.2010

Maris, E., & Oostenveld, R. (2007). Nonparametric statistical testing of EEG- and MEG-data. *Journal of Neuroscience Methods*. https://doi.org/10.1016/j.jneumeth.2007.03.024

Matthews, W. J., & Gheorghiu, A. I. (2016). Repetition, expectation, and the perception of time. *Current Opinion in Behavioral Sciences*. https://doi.org/10.1016/j.cobeha.2016.02.019

McLelland, D., Lavergne, L., & VanRullen, R. (2016). The phase of ongoing EEG oscillations predicts the amplitude of peri-saccadic mislocalization. *Scientific Reports*. https://doi.org/10.1038/srep29335

Medendorp, W. P., Kramer, G. F. I., Jensen, O., Oostenveld, R., Schoffelen, J. M., & Fries, P. (2007). Oscillatory activity in human parietal and occipital cortex shows hemispheric lateralization and memory effects in a delayed double-step saccade task. *Cerebral Cortex*. https://doi.org/10.1093/cercor/bhl145

Mégevand, P., & Seeck, M. (2018). Electroencephalography, magnetoencephalography and source localization: their value in epilepsy. *Current Opinion in Neurology*, *31*(2). Retrieved from https://journals.lww.com/co-neurology/Fulltext/2018/04000/Electroencephalography,_magnetoencephalography_and.12.aspx

Melcher, D. (2007). Predictive remapping of visual features precedes saccadic eye movements. *Nature Neuroscience*. https://doi.org/10.1038/nn1917

Melcher, D., & Colby, C. L. (2008). Trans-saccadic perception. *Trends in Cognitive Sciences*. https://doi.org/10.1016/j.tics.2008.09.003

Morrone, M. C., Ross, J., & Burr, D. (2005). Saccadic eye movements cause compression of time as well as space. *Nature Neuroscience*, *8*(7), 950–954. https://doi.org/10.1038/nn1488

Mort, D. J., Perry, R. J., Mannan, S. K., Hodgson, T. L., Anderson, E., Quest, R., … Kennard, C. (2003). Differential cortical activation during voluntary and reflexive

saccades in man. *NeuroImage*, *18*(2), 231–246. https://doi.org/https://doi.org/10.1016/S1053-8119(02)00028-9

Muldoon, S. F., Bridgeford, E. W., & Bassett, D. S. (2016). Small-World Propensity and Weighted Brain Networks. *Scientific Reports*, *6*(1), 22057. https://doi.org/10.1038/srep22057

Newman, M. (2008). The physics of networks. *Physics Today*. https://doi.org/10.1063/1.3027989

Nunez, P. L., Srinivasan, R., Westdorp, A. F., Wijesinghe, R. S., Tucker, D. M., Silberstein, R. B., & Cadusch, P. J. (1997). EEG coherency I: Statistics, reference electrode, volume conduction, Laplacians, cortical imaging, and interpretation at multiple scales. *Electroencephalography and Clinical Neurophysiology*. https://doi.org/10.1016/S0013-4694(97)00066-7

Paré, M., & Wurtz, R. H. (2001). Progression in Neuronal Processing for Saccadic Eye Movements From Parietal Cortex Area LIP to Superior Colliculus. *Journal of Neurophysiology*, *85*(6), 2545–2562. https://doi.org/10.1152/jn.2001.85.6.2545

Pascual-Marqui, R. D. (2002). Standardized low-resolution brain electromagnetic tomography (sLORETA): Technical details. *Methods and Findings in Experimental and Clinical Pharmacology*.

Pascual-Marqui, Roberto D. (2007). *Instantaneous and lagged measurements of linear and nonlinear dependence between groups of multivariate time series: frequency decomposition*. 1–18. Retrieved from http://arxiv.org/abs/0711.1455

Pascual-Marqui, Roberto D., Lehmann, D., Koukkou, M., Kochi, K., Anderer, P., Saletu, B., … Kinoshita, T. (2011). Assessing interactions in the brain with exact low-resolution electromagnetic tomography. *Philosophical Transactions of the Royal Society A: Mathematical, Physical and Engineering Sciences*. https://doi.org/10.1098/rsta.2011.0081

Paus, T. (1996). Location and function of the human frontal eye-field: A selective review. *Neuropsychologia*, *34*(6), 475–483.

https://doi.org/https://doi.org/10.1016/0028-3932(95)00134-4

Pedersen, M., Omidvarnia, A. H., Walz, J. M., & Jackson, G. D. (2015). Increased segregation of brain networks in focal epilepsy: An fMRI graph theory finding. *NeuroImage: Clinical*, *8*, 536–542. https://doi.org/https://doi.org/10.1016/j.nicl.2015.05.009

Pesaran, B., Pezaris, J. S., Sahani, M., Mitra, P. P., & Andersen, R. A. (2002). Temporal structure in neuronal activity during working memory in macaque parietal cortex. *Nature Neuroscience*, *5*(8), 805–811. https://doi.org/10.1038/nn890

Ploner, C. J., Gaymard, B. M., Rivaud-Péchoux, S., & Pierrot-Deseilligny, C. (2005). The prefrontal substrate of reflexive saccade inhibition in humans. *Biological Psychiatry*. https://doi.org/10.1016/j.biopsych.2005.02.017

Powell, K. D., & Goldberg, M. E. (2000). Response of neurons in the lateral intraparietal area to a distractor flashed during the delay period of a memory-guided saccade. *Journal of Neurophysiology*. https://doi.org/10.1152/jn.2000.84.1.301

Rajkowska, G., & Goldman-Rakic, P. S. (1995). Cytoarchitectonic Definition of Prefrontal Areas in the Normal Human Cortex: II. Variability in Locations of Areas 9 and 46 and Relationship to the Talairach Coordinate System. *Cerebral Cortex*, *5*(4), 323–337. https://doi.org/10.1093/cercor/5.4.323

Ross, J., Morrone, M. C., Goldberg, M. E., & Burr, D. C. (2001). Changes in visual perception at the time of saccades. *Trends in Neurosciences*, *24*(2), 113–121. https://doi.org/https://doi.org/10.1016/S0166-2236(00)01685-4

Rubinov, M., & Sporns, O. (2010). Complex network measures of brain connectivity: Uses and interpretations. *NeuroImage*. https://doi.org/10.1016/j.neuroimage.2009.10.003

Rubinov, M., & Sporns, O. (2011). Weight-conserving characterization of complex functional brain networks. *NeuroImage*. https://doi.org/10.1016/j.neuroimage.2011.03.069

Rushworth, M. F. S., Behrens, T. E. J., & Johansen-Berg, H. (2006). Connection

Patterns Distinguish 3 Regions of Human Parietal Cortex. *Cerebral Cortex*, *16*(10), 1418–1430. https://doi.org/10.1093/cercor/bhj079

Sadeh, M., Sajad, A., Wang, H., Yan, X., & Crawford, J. D. (2018). The influence of a memory delay on spatial coding in the superior colliculus: Is visual always visual and motor always motor? *Frontiers in Neural Circuits*. https://doi.org/10.3389/fncir.2018.00074

Sajad, A., Sadeh, M., Yan, X., Wang, H., & Crawford, J. D. (2016). Transition from target to gaze coding in primate frontal eye field during memory delay and memory-motor transformation. *ENeuro*. https://doi.org/10.1523/ENEURO.0040-16.2016

Sapir, A., Hayes, A., Henik, A., Danziger, S., & Rafal, R. (2004). Parietal lobe lesions disrupt saccadic remapping of inhibitory location tagging. *Journal of Cognitive Neuroscience*. https://doi.org/10.1162/089892904323057245

Saramäki, J., Kivelä, M., Onnela, J.-P., Kaski, K., & Kertész, J. (2007). Generalizations of the clustering coefficient to weighted complex networks. *Physical Review E*, *75*(2), 27105. https://doi.org/10.1103/PhysRevE.75.027105

Schall, J. D., & Hanes, D. P. (1993). Neural basis of saccade target selection in frontal eye field during visual search. *Nature*. https://doi.org/10.1038/366467a0

Schall, J. D., Hanes, D. P., Thompson, K. G., & King, D. J. (1995). Saccade target selection in frontal eye field of macaque. I. Visual and premovement activation. *Journal of Neuroscience*. https://doi.org/10.1523/jneurosci.15-10-06905.1995

Shannon, C. E., & warren weaver. (1949). The mathematical theory ofcommunication. *THE UNIVERSITY OF ILLINOIS PRESS*. https://doi.org/10.1145/584091.584093

Shioiri, S., & Cavanagh, P. (1989). Saccadic suppression of low-level motion. *Vision Research*, *29*(8), 915–928. https://doi.org/https://doi.org/10.1016/0042-6989(89)90106-5

Simon, O., Mangin, J.-F., Cohen, L., Le Bihan, D., & Dehaene, S. (2002). Topographical Layout of Hand, Eye, Calculation, and Language-Related Areas in the Human Parietal Lobe. *Neuron*, *33*(3), 475–487.

https://doi.org/https://doi.org/10.1016/S0896-6273(02)00575-5

Sjoerds, Z., Stufflebeam, S. M., Veltman, D. J., Van den Brink, W., Penninx, B. W. J. H., & Douw, L. (2017). Loss of brain graph network efficiency in alcohol dependence. *Addiction Biology*, *22*(2), 523–534. https://doi.org/https://doi.org/10.1111/adb.12346

Sommer, M. A., & Wurtz, R. H. (2000). Composition and Topographic Organization of Signals Sent From the Frontal Eye Field to the Superior Colliculus. *Journal of Neurophysiology*, *83*(4), 1979–2001. https://doi.org/10.1152/jn.2000.83.4.1979

Spielman, D. A. (2007). Spectral graph theory and its applications. *Proceedings - Annual IEEE Symposium on Foundations of Computer Science, FOCS*. https://doi.org/10.1109/FOCS.2007.4389477

Sporns, O. (2013). Network attributes for segregation and integration in the human brain. *Current Opinion in Neurobiology*, *23*(2), 162–171. https://doi.org/https://doi.org/10.1016/j.conb.2012.11.015

Sporns, O. (2014). Contributions and challenges for network models in cognitive neuroscience. *Nature Neuroscience*. https://doi.org/10.1038/nn.3690

Stam, C. J. (2014). Modern network science of neurological disorders. *Nature Reviews Neuroscience*, *15*(10), 683–695. https://doi.org/10.1038/nrn3801

Stam, C. J., & Reijneveld, J. C. (2007). Graph theoretical analysis of complex networks in the brain. *Nonlinear Biomedical Physics*. https://doi.org/10.1186/1753-4631-1-3

Stancák, A., & Pfurtscheller, G. (1996). Event-related desynchronisation of central beta-rhythms during brisk and slow self-paced finger movements of dominant and nondominant hand. *Cognitive Brain Research*. https://doi.org/10.1016/S0926-6410(96)00031-6

Staudigl, T., Hartl, E., Noachtar, S., Doeller, C. F., & Jensen, O. (2017). Saccades are phase-locked to alpha oscillations in the occipital and medial temporal lobe during successful memory encoding. *PLoS Biology*. https://doi.org/10.1371/journal.pbio.2003404

Strotzer, M. (2009). One century of brain mapping using Brodmann areas. *Clinical Neuroradiology*. https://doi.org/10.1007/s00062-009-9002-3

Subramanian, J., & Colby, C. L. (2014). Shape selectivity and remapping in dorsal stream visual area LIP. *Journal of Neurophysiology*. https://doi.org/10.1152/jn.00841.2011

Thiele, A., Henning, P., Kubischik, M., & Hoffmann, K. P. (2002). Neural mechanisms of saccadic suppression. *Science*. https://doi.org/10.1126/science.1068788

Tzagarakis, C., Ince, N. F., Leuthold, A. C., & Pellizzer, G. (2010). Beta-band activity during motor planning reflects response uncertainty. *Journal of Neuroscience*. https://doi.org/10.1523/JNEUROSCI.6026-09.2010

Umeno, M. M., & Goldberg, M. E. (1997). Spatial processing in the monkey frontal eye field. I. Predictive visual responses. *Journal of Neurophysiology*. https://doi.org/10.1152/jn.1997.78.3.1373

van den Heuvel, M. P., Stam, C. J., Boersma, M., & Hulshoff Pol, H. E. (2008). Small-world and scale-free organization of voxel-based resting-state functional connectivity in the human brain. *NeuroImage*. https://doi.org/10.1016/j.neuroimage.2008.08.010

Verfaellie, M., Schacter, D. L., Dobbins, I. G., & Schnyer, D. M. (2004). Cortical activity reductions during repetition priming can result from rapid response learning. *Nature*, *428*(6980), 316–319.

Vesia, M., & Crawford, J. D. (2012). Specialization of reach function in human posterior parietal cortex. *Experimental Brain Research*, *221*(1), 1–18. https://doi.org/10.1007/s00221-012-3158-9

Vesia, M., Prime, S. L., Yan, X., Sergio, L. E., & Crawford, J. D. (2010). Specificity of Human Parietal Saccade and Reach Regions during Transcranial Magnetic Stimulation. *The Journal of Neuroscience*, *30*(39), 13053 LP – 13065. https://doi.org/10.1523/JNEUROSCI.1644-10.2010

Wang, D., Liu, Z., Tao, Y., Chen, W., Chen, B., Wang, Q., … Wang, G. (2021).

Improvement in EEG Source Imaging Accuracy by Means of Wavelet Packet Transform and Subspace Component Selection. *IEEE Transactions on Neural Systems and Rehabilitation Engineering*, *29*, 650–661. https://doi.org/10.1109/TNSRE.2021.3064665

Watts, D. J., & Strogatz, S. H. (1998). Collective dynamics of “small-world” networks. *Nature*. https://doi.org/10.1038/30918

Wilf, H. S. (1967). The Eigenvalues of a Graph and Its Chromatic Number. *Journal of the London Mathematical Society*, *s1-42*(1), 330–332. https://doi.org/https://doi.org/10.1112/jlms/s1-42.1.330

Xia, M., Wang, J., & He, Y. (2013). BrainNet Viewer: A Network Visualization Tool for Human Brain Connectomics. *PLOS ONE*, *8*(7), e68910. Retrieved from https://doi.org/10.1371/journal.pone.0068910